AFRL-RX-WP-JA-2017-0299

REDOX LIQUID PHASE EXFOLIATION OF LAYERED TRANSITION METAL DICHALCOGENIDES (POSTPRINT)

Ali Jawaid, Justin Che, Lawrence F. Drummy, John Bultman, Adam Waite, Ming-Siao Hsiao, Richard A. Vaia

AFRL/RX

12 January 2017
Interim Report

(STINFO COPY)

AIR FORCE RESEARCH LABORATORY
MATERIALS AND MANUFACTURING DIRECTORATE
WRIGHT-PATTERSON AIR FORCE BASE, OH 45433-7750
AIR FORCE MATERIEL COMMAND
UNITED STATES AIR FORCE

REPORT DOCUMENTATION PAGE

Form Approved
OMB No. 0704-0188

1. REPORT DATE *(DD-MM-YY)*	2. REPORT TYPE	3. DATES COVERED *(From - To)*
12 January 2017	Interim	8 September 2014 – 12 December 2016

4. TITLE AND SUBTITLE
REDOX LIQUID PHASE EXFOLIATION OF LAYERED TRANSITION METAL DICHALCOGENIDES (POSTPRINT)

5a. CONTRACT NUMBER
FA8650-15-D-5405-0002

5b. GRANT NUMBER

5c. PROGRAM ELEMENT NUMBER

6. AUTHOR(S)
Ali Jawaid, Justin Che, Lawrence F. Drummy, John Bultman, Adam Waite, Ming-Siao Hsiao, and Richard A. Vaia – AFRL/RX

5d. PROJECT NUMBER

5e. TASK NUMBER 0002

5f. WORK UNIT NUMBER
X0YE

7. PERFORMING ORGANIZATION NAME(S) AND ADDRESS(ES)
AFRL/RX Wright-Patterson AFB,
Dayton, OH 45433

8. PERFORMING ORGANIZATION REPORT NUMBER

9. SPONSORING/MONITORING AGENCY NAME(S) AND ADDRESS(ES)
Air Force Research Laboratory
Materials and Manufacturing Directorate
Wright-Patterson Air Force Base, OH 45433-7750
Air Force Materiel Command
United States Air Force

10. SPONSORING/MONITORING AGENCY ACRONYM(S)
AFRL/RXAS

11. SPONSORING/MONITORING AGENCY REPORT NUMBER(S)
AFRL-RX-WP-JA-2017-0299

12. DISTRIBUTION/AVAILABILITY STATEMENT
Distribution Statement A. Approved for public release: distribution unlimited.

13. SUPPLEMENTARY NOTES
PA Case Number: 88ABW-2017-0107; Clearance Date: 12 Jan 2017. This document contains color. Journal article published in ACS Nano, Vol. 11, No. 1, 29 Dec 2016. © 2016 American Chemical Society. The U.S. Government is joint author of the work and has the right to use, modify, reproduce, release, perform, display, or disclose the work.
The final publication is available at DOI: 10.1021/acsnano.6b06922

14. ABSTRACT *(Maximum 200 words)*
Layered transition metal dichalcogenides (TMDs) are an emerging class of 2-dimensional materials due to their diverse property suite, which range from semiconducting and semimetallic to metallic and superconducting.1 Their lamellar structure consists of a transition metal layer (M) sandwiched between two chalcogen layers (X) with strong M-X intralayer bonding. These layers are separated by a weak van der waals gap. At the few- to mono-layer limit, coupling between layers is reduced, in-plane confinement dominates, and the band structure changes. This affords unique opportunities for chemical sensing, catalysis, spintronics, single-photon emission, infrared optics, nanocomposites, coatings, and printable inks for nanoelectronics.2–5 Thus, a suite of processing methods have evolved to satisfy application-specific requirements, such as defect density, scale, cost, and integration. Top-down exfoliation of powders affords large volume use and compliments molecular-based monolayer growth for micro-fabricated devices.

15. SUBJECT TERMS
liquid-phase exfoliation; MoS2; redox exfoliation; surface oxidation; surface reactivity; transition metal dichalcogenides

16. SECURITY CLASSIFICATION OF:			17. LIMITATION OF ABSTRACT:	18. NUMBER OF PAGES	19a. NAME OF RESPONSIBLE PERSON (Monitor)
a. REPORT	b. ABSTRACT	c. THIS PAGE			Lawrence Brott
Unclassified	Unclassified	Unclassified	SAR	35	19b. TELEPHONE NUMBER *(Include Area Code)* (937) 255-9157

Redox Liquid Phase Exfoliation of Layered Transition Metal Dichalcogenides

*Ali Jawaid, Justin Che, Lawrence F. Drummy, John Bultman, Adam Waite, Ming-Siao Hsiao, Richard A. Vaia**

Materials and Manufacturing Directorate, Air Force Research Laboratory,

Wright-Patterson AFB, Ohio 45433-7702

*richard.vaia@us.af.mil, Phone number 937-785-9209

Table of Contents:

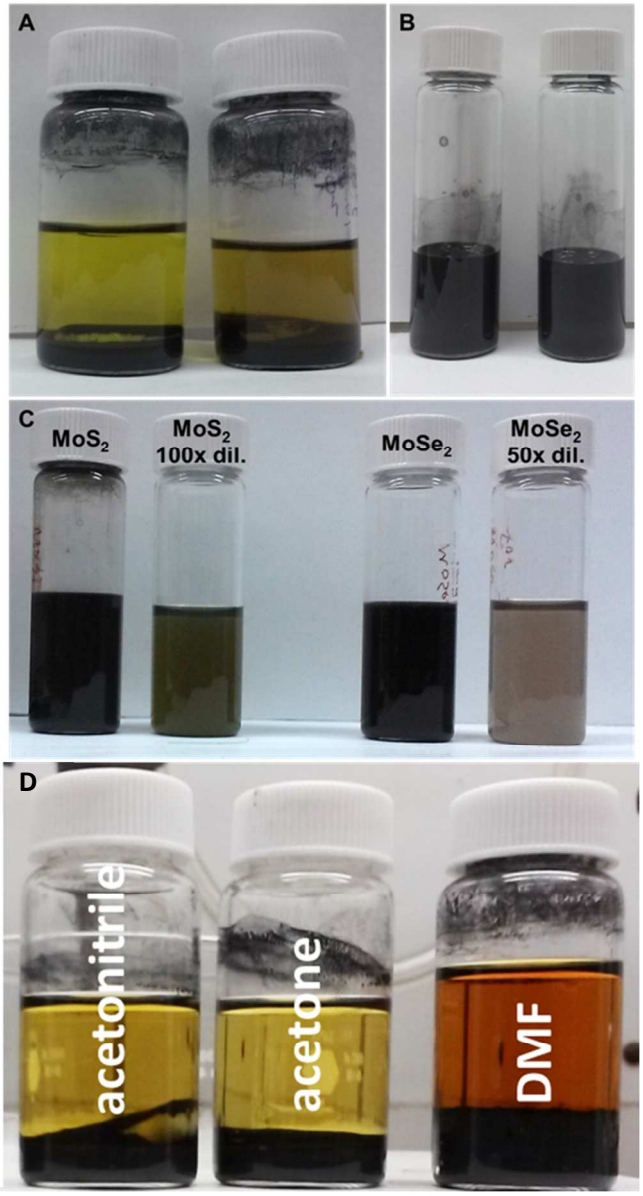

Figure S1. **A)** Picture of MoS_2 in CH_3CN (ACN, 100 mg, 10 mL) after addition of 5 mmol of cumene hydroperoxide (CHP). The flakes sediment immediately after stir is removed, and the supernatant contains dissolution peroxo-molybdenum species. Image taken after stir was removed for 5 minutes. **B)** After concentrating the solution (4 mL total), and addition of $NaBH_4$ (0.10 M, 400 μL) at 0^oC, stable suspensions of MoS_2 are obtained. The suspensions contain both large/thick and exfoliated flakes. Image is taken after stir was removed for 24 hours. **C)** Image of MoS_2 and $MoSe_2$ after centrifugation at 1500 RPM for 45 minutes. The supernatant contains exfoliated flakes. **D)** Addition of CHP in other solvents also results in generation of a soluble species, suggesting this method is applicable for many solvents.

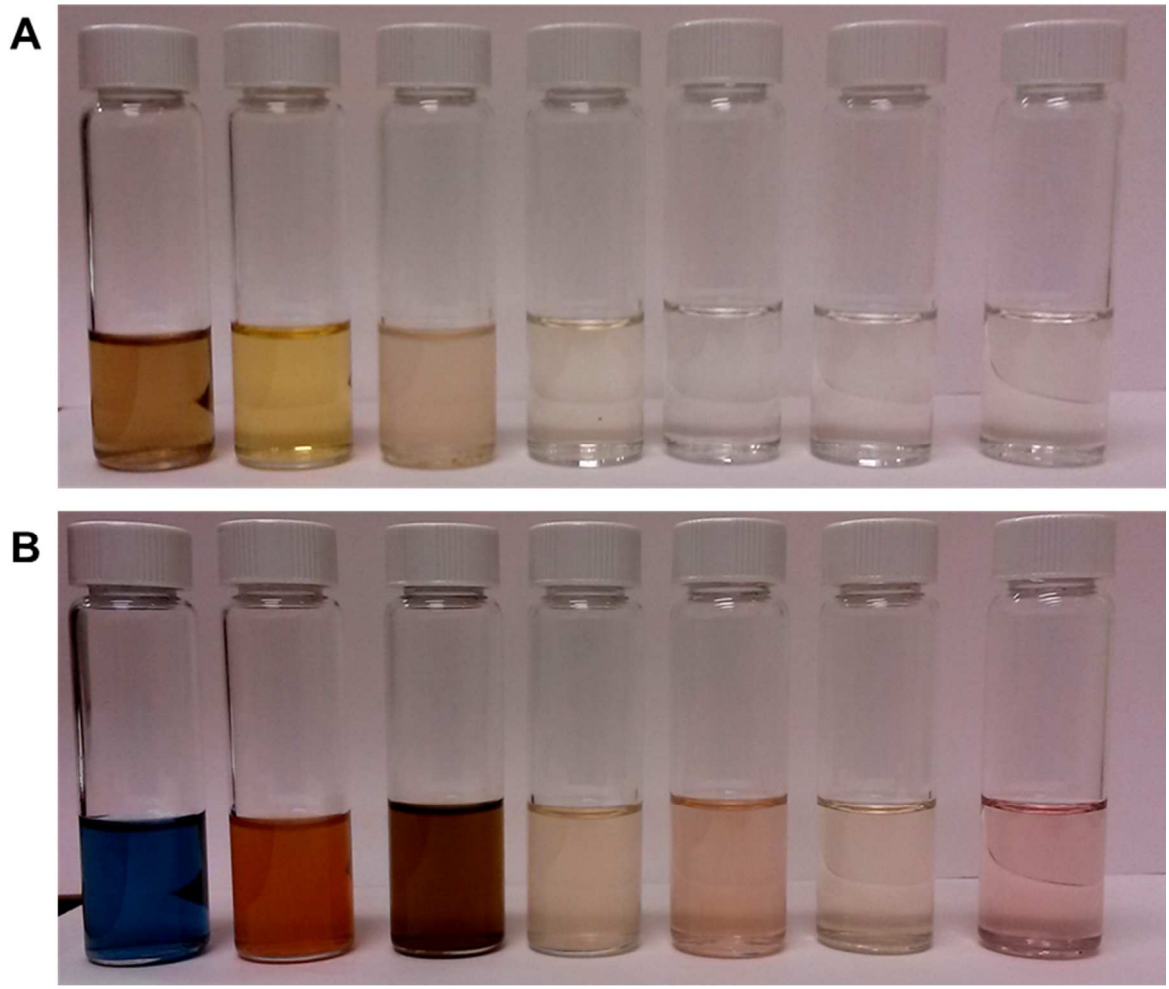

Figure S2. **A)** Supernatants isolated from TMDs after oxidation with cumene hydroperoxide (CHP). Discoloration is present in all vials, indicating partial dissolution of TMD powders. **B)** After addition of dilute aqueous $NaBH_4$ (0.010 M, 100 μL), a colormetric response is observed (from left to right) for MoS_2, $MoSe_2$, $MoTe_2$, WS_2, WSe_2, $NbSe_2$, and ReS_2. The characteristic blue color seen in MoS_2 dispersions is indication of anionic polyoxometalates (POMs) formed in-situ with mixed Mo^{V}-Mo^{VI} valency.[1,2] Thus, partial reduction of dissolution products after oxidation results in POM formation. It can be reasoned that this process is occurring in other TMDs, as many transition metals are known to form POM species.[3–5]

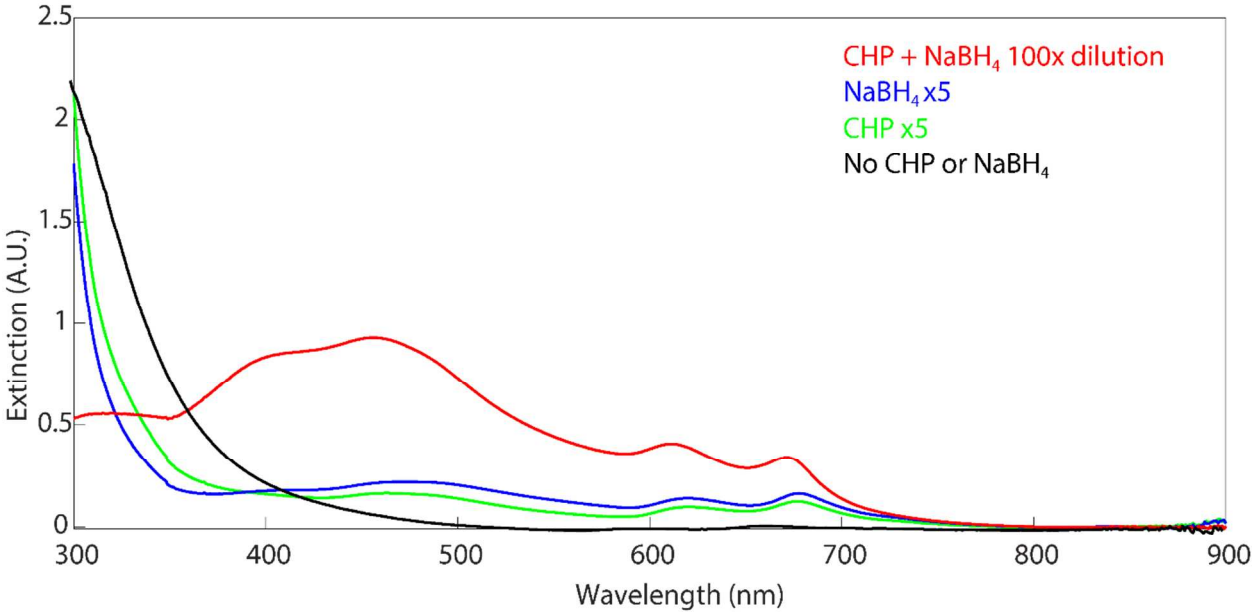

Figure S3. Extinction spectra of 100 mg MoS_2 (0.625 mmol) suspended in 10 mL CH_3CN (ACN) with the addition of CHP and $NaBH_4$ (red), with only $NaBH_4$ (no CHP, blue), with only CHP (no $NaBH_4$, green), and without CHP or $NaBH_4$ (black). Small quantities of MoS_2 are exfoliated with only the addition of oxidant (CHP) or reductant ($NaBH_4$). However, if the redox reaction is carried out, MoS_2 flakes exfoliate into solution readily. The MoS_2 sheets in solution with just CHP or $NaBH_4$ have a peak at 680 nm, indicating very thick flakes. However, after CHP/$NaBH_4$ co-addition, the thickness of the flakes decreases (peak at 670 nm) with a significant increase in yields. Curves for $NaBH_4$, CHP are multiplied by 5x to resolve spectral features (i.e. CHP + $NaBH_4$ is 500x more intense).

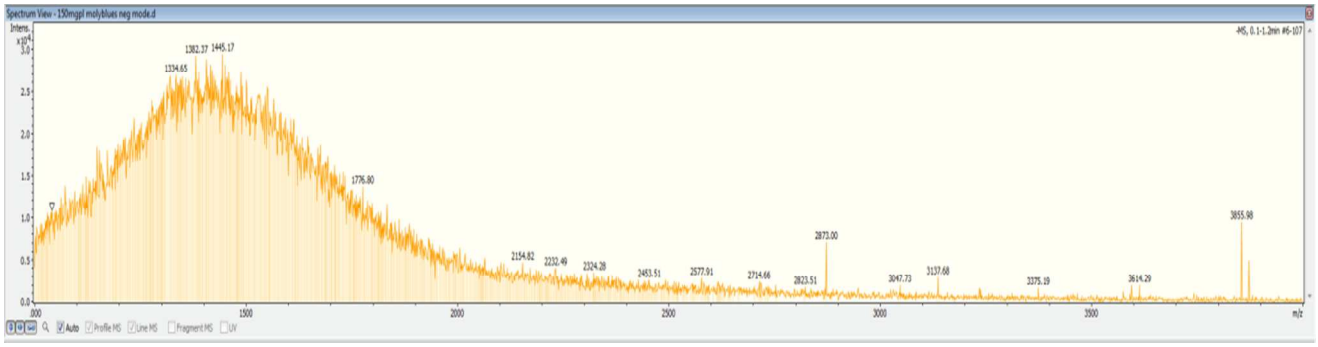

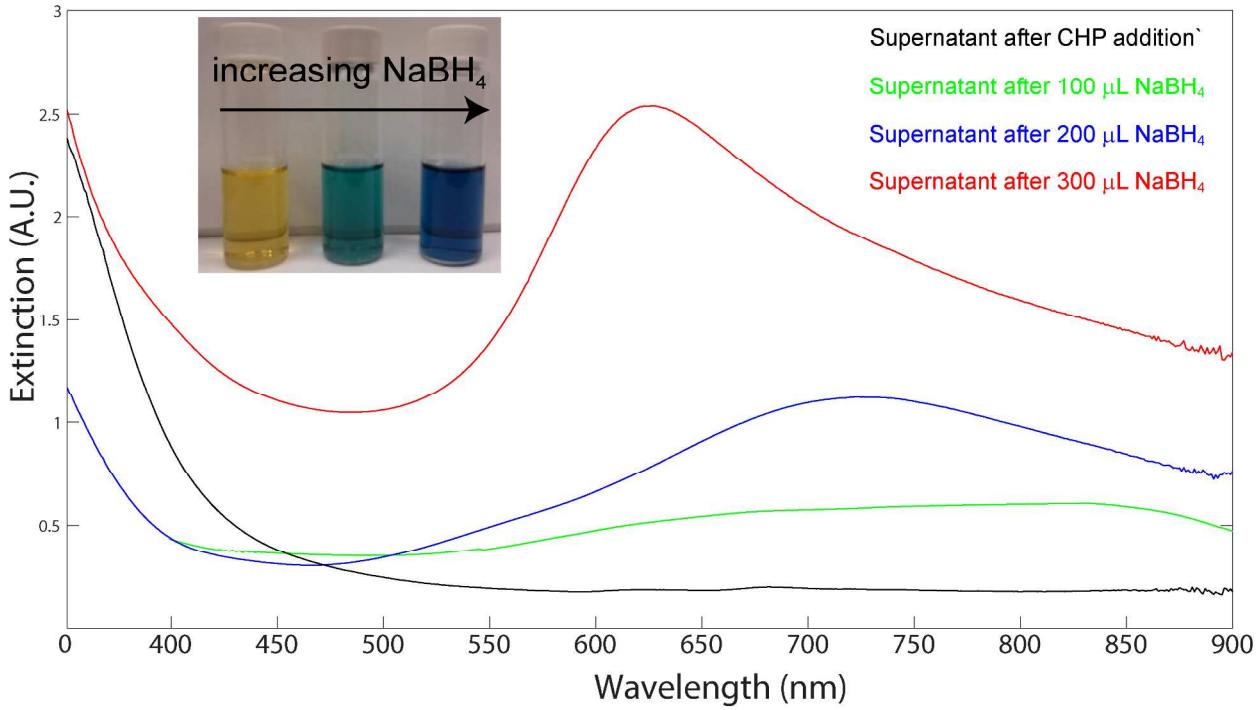

Figure S4. Mass spectra of isolated supernatant from MoS_2 after addition of 300 mL of $NaBH_4$ indicating formation of large species in solution (blue vial). UV-Vis analysis of the isolated supernatant after addition of CHP (black UV-Vis curve, yellow solution in digital image) is consistent with peroxo-molybdenum species.[6,7] As the solution is titrated with $NaBH_4$, the colormetric response indicates formation of mixed valent Mo^{VI}-Mo^{V} species, consistent with POMo formation.[2,8]

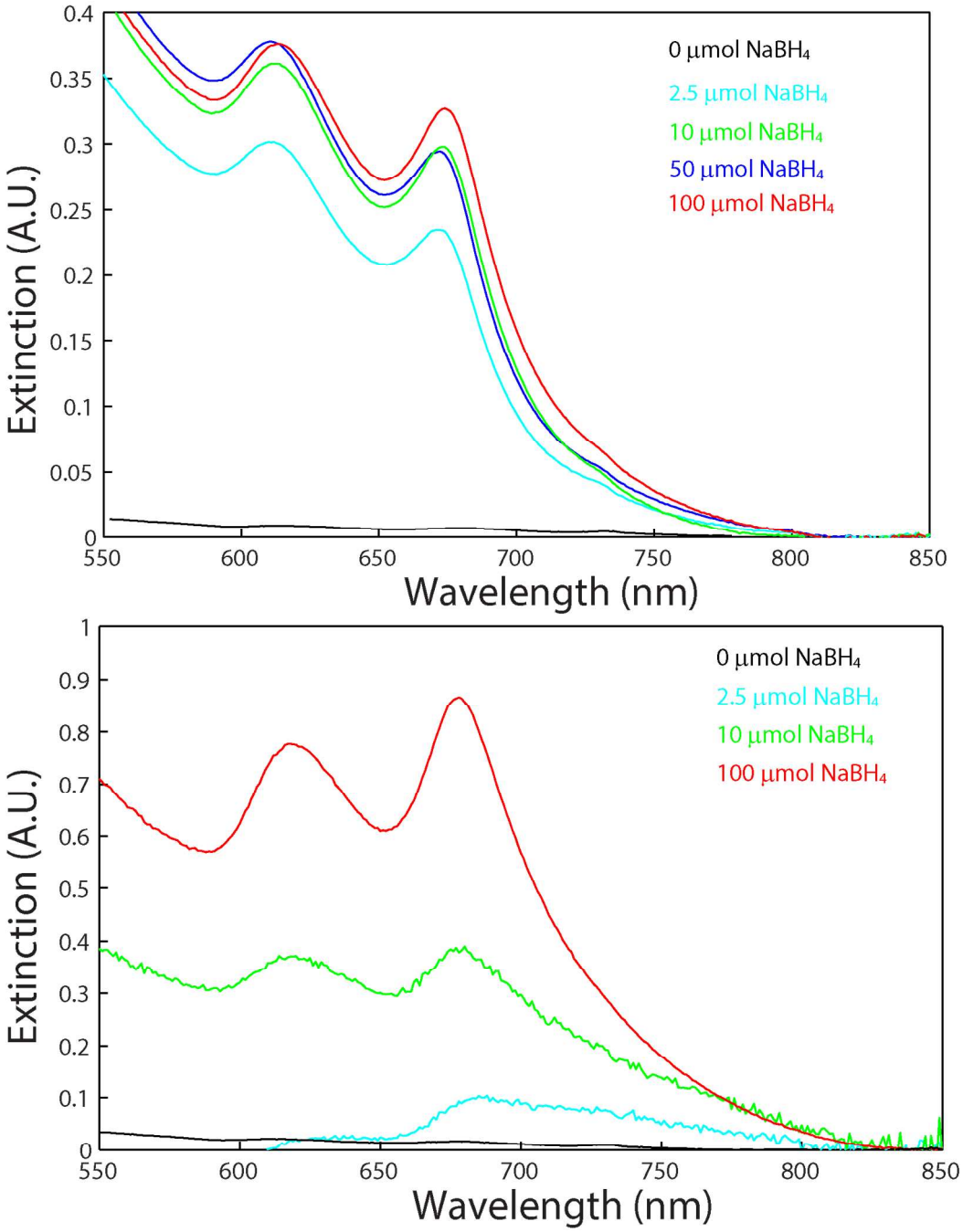

Figure S5. Extinction spectra of exfoliated MoS_2 (0.1875 mmol MoS_2, 10 mL solvent) after oxidation with CHP (1.5 mmol, 8:1 CHP:MoS_2) and subsequent incremental addition of $NaBH_4$ in **A)** Acetonitrile and **B)** Acetone. After the indicated amount of $NaBH_4$ was added, the solution was allowed to stir for 1 hr before collection of the suspension that was centrifuged at 1500 RPM (30 min). The resultant supernatant was analyzed via UV-Vis spectroscopy. Initially (i.e. no $NaBH_4$), the supernatant contains no exfoliated MoS_2 flakes. After addition of $NaBH_4$, MoS_2 slowly exfoliates, until saturation occurs after c.a. 100 μmol.

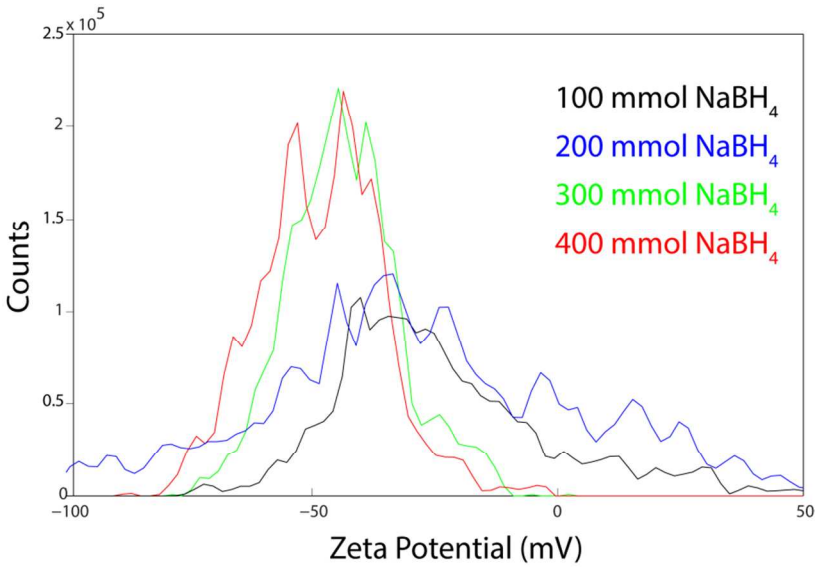

Figure S6a. Zeta potential of MoS_2 (100 mg, 10 mL CH_3CN) after oxidation with CHP (3.2 mol) and subsequent incremental addition of $NaBH_4$. Initially, the zeta potential is broad. After incremental additional of $NaBH_4$, the zeta potential slowly shifts to more negative values, consistent with the proposed mechanism of POM adsorption and charging.

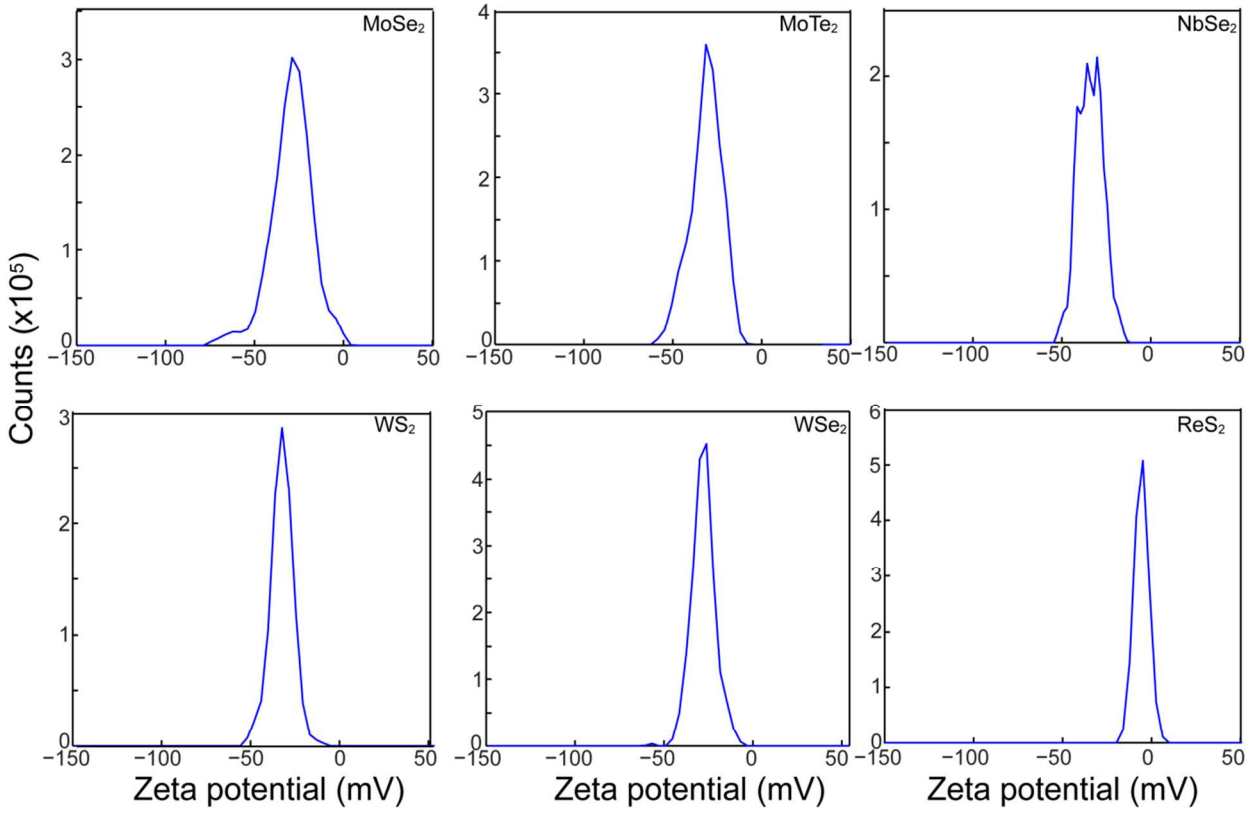

Figure S6b. Zeta potential measurements of all TMDs confirm a negative surface charge, consistent with the proposed mechanism of anionic POM adsorption.

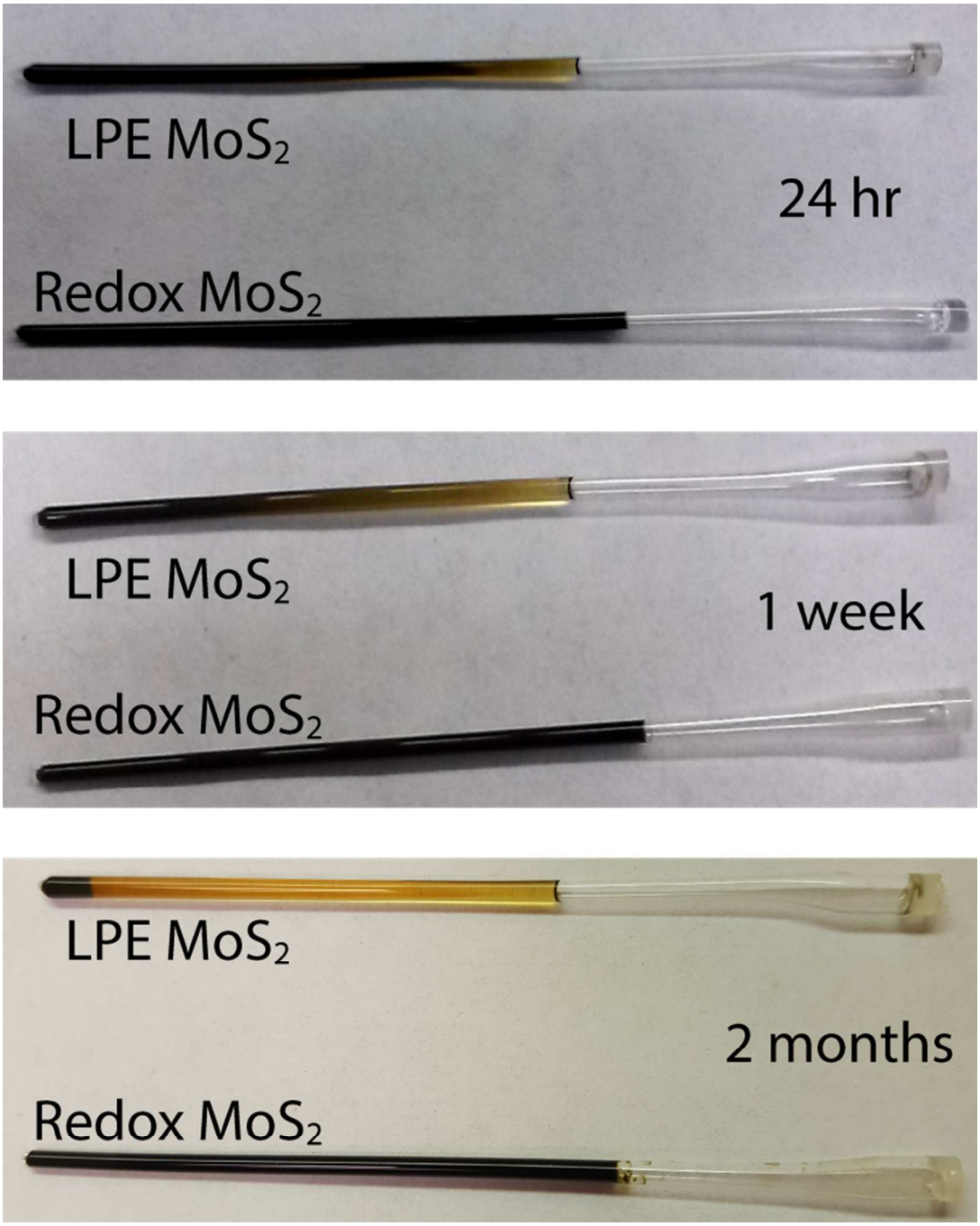

Figure S7. Optical images of MoS_2 prepared via liquid phase exfoliation (90 hrs, probe-tip sonication @ 127.5 W)) and redox exfoliation methods deposited in quartz capillaries for solution XRD. Redox exfoliated samples showed no sign of sedimentation, even after 2 months, whereas probe-tip sonicated samples show phase separation after 24 hours, and completely sediment within 2 months.

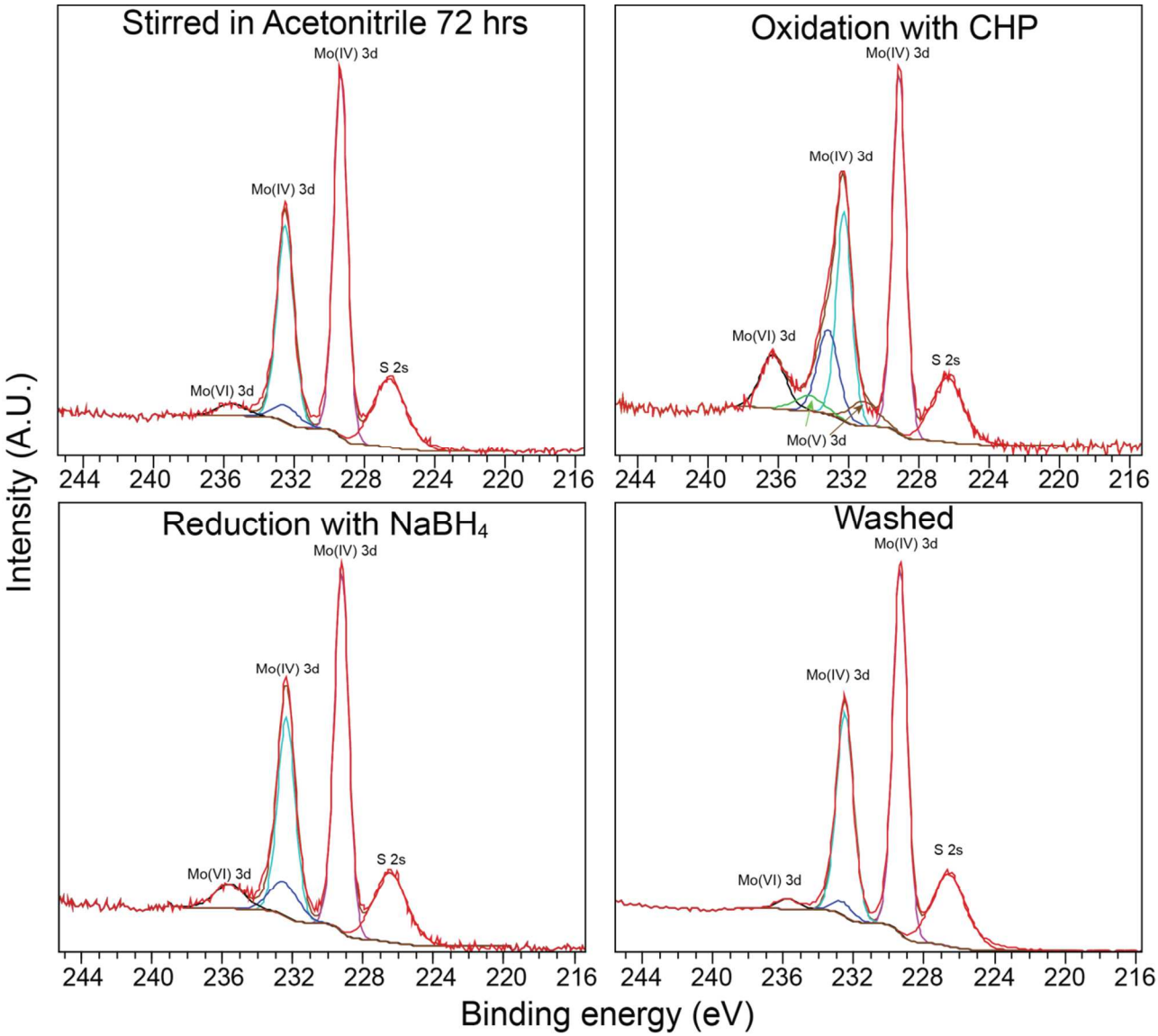

	Mo(VI)	Mo(V)	Mo(IV)	S	Mo:S	MoIV:S
Stir 72 hr	3.96	N/A	33.51	62.53	0.60	0.53
Oxidation	12.10	4.34	31.58	51.98	0.92	0.61
Reduction	6.64	N/A	33.96	59.41	0.68	0.57
Washed	1.95	N/A	34.19	63.86	0.57	0.54

Figure S8. XPS spectra of MoS_2 during different stages of redox reaction. Initially, after stirring in acetonitrile, the supernatant becomes slightly discolored (blue) indicating the dissolution of MoS_2 species. This occurs without the addition of oxidizing agent, consistent with a recent report showing dissolution kinetics of MoS_2 flakes. These species are consistent with POMo with Mo^{VI} valency. After subsequent addition of CHP to these flakes, the abundance of Mo^{VI} species increases, suggesting surface oxidation of flakes. However, because the Mo^{IV}:S ratio remains relatively constant (0.53 – 0.61), the oxidation likely doesn't destroy the integrity of the MoS_2 basal surface. After reduction, the Mo^{VI} species abundance is reduced, where upon subsequent washing with fresh solvent after centrifugation and reconstitution cycles, the Mo^{VI} species (likely on the surface) can be washed out of the exfoliated flakes.

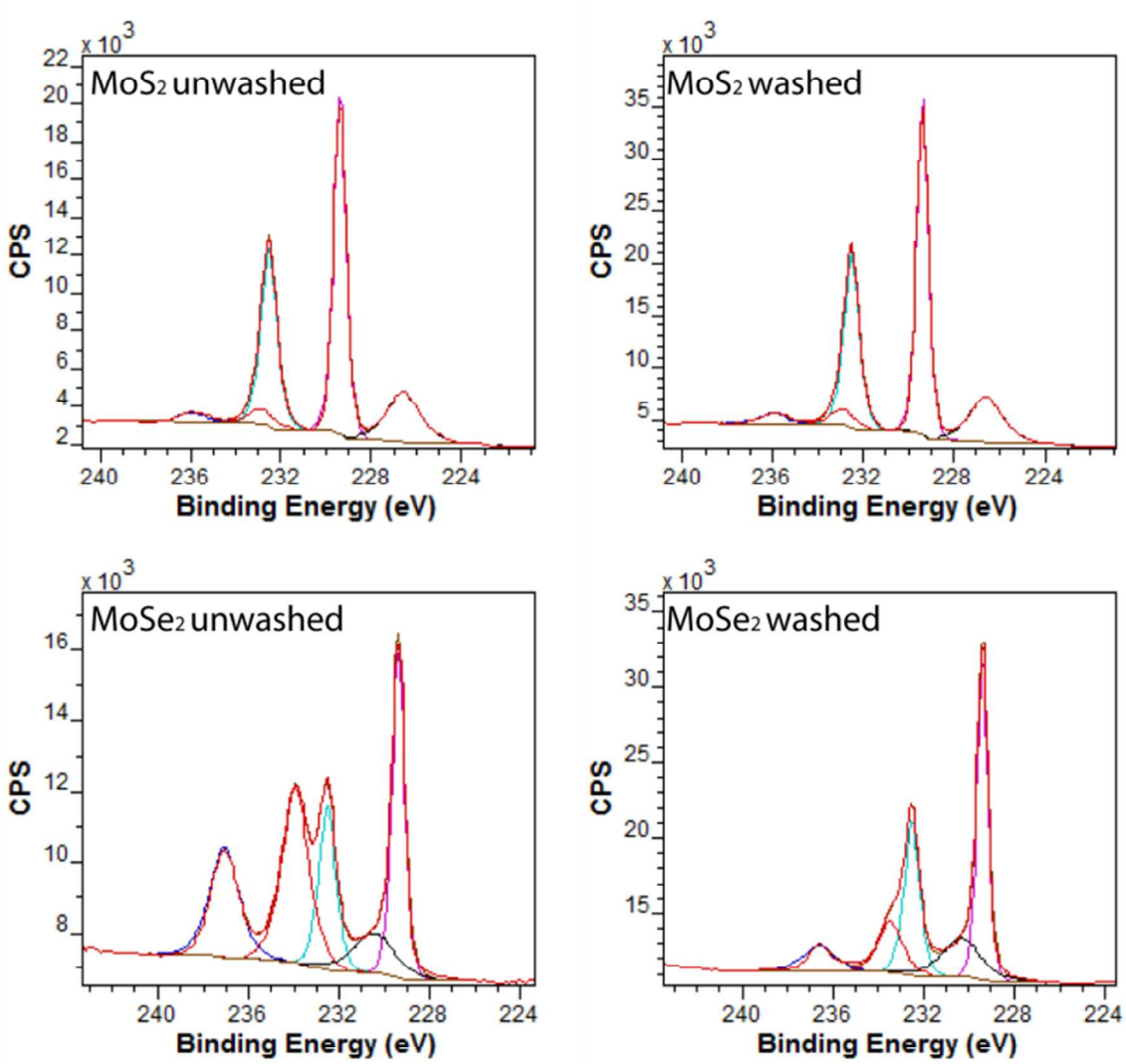

TMD	% abundance Mo^{IV}	% abundance Mo^{VI}	Mo^{IV}:X	Mo:X
MoS_2 Unwashed	32.7 ± 0.20	4.44 ± 1.59	0.52 ± 0.00	0.65 ± 0.00
MoS_2 washed	33.1 ± 0.15	3.23 ± 0.25	0.52 ± 0.00	0.62 ± 0.00
$MoSe_2$ Unwashed	$23.4. \pm 1.74$	16.5 ± 7.15	0.39 ± 0.02	0.62 ± 0.01
$MoSe_2$ washed	24.0 ± 0.85	8.30 ± 0.44	0.35 ± 0.01	0.65 ± 0.01

Figure S9. XPS spectra of Mo_{3d} (Mo^{VI}, 236.0 eV; Mo^{IV} 234.2 eV) region for MoS_2 and $MoSe_2$ before and after washing cycles. Washing cycles were performed by centrifuging the exfoliated dispersion at 10000 RPM for 15 minutes, discarding the supernatant, and re-suspending the flakes in fresh, anhydrous solvent. The presence of expected Mo^{VI} species is observed in both MoS_2 (4.5% abundance) and $MoSe_2$ (16.5% abundance) prior to washing. After washing, the abundance decreases in MoS_2 samples by 33% (3.23% abundance Mo^{VI}), and 52% (8.30% Mo^{VI}) in $MoSe_2$. The Mo^{IV}:S ratio for MoS_2 was 1:2, indicating the presence of pristine TMD, with a Mo^{VI} species that can be removed by washing. In $MoSe_2$, the Mo^{IV}:Se ratio is 0.39, which may be due to incorporation of Se in the POMo matrix[9], resulting in deviations from the 1:2 ratio expected. In both cases, the total Mo:X ratio is much larger than the expected 0.50 (0.62 MoS_2, 0.65 $MoSe_2$), indicating that extra Mo is present in the prepared films. After washing, the Mo^{IV} abundance does not decrease, whereas the Mo^{VI} is reduced by 50%, suggesting the Mo^{VI} signal is not associated with the exfoliated TMD.

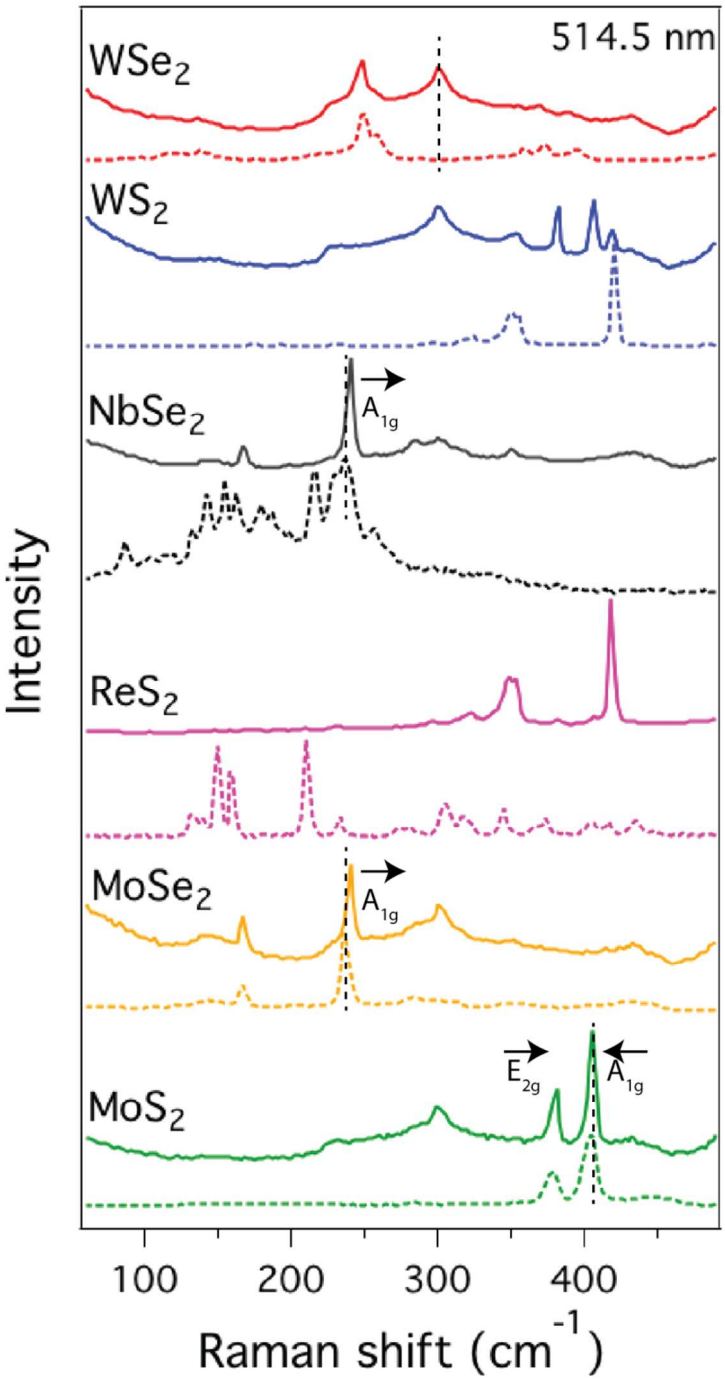

Figure S10. Raman spectra of few layer and bulk TMDs. MoS_2 shows characteristic shifts in the A_{1g} – E_{2g} energy levels (~ 2 cm^{-1}) due to reduction in thickness (black dotted line). Similar shifts are seen in $NbSe_2$, $MoSe_2$, as well as new low-dimensional modes appearing in $MoSe_2$ and WSe_2. These data suggest reduction of dimensionality in exfoliated TMDs compared to bulk powders.

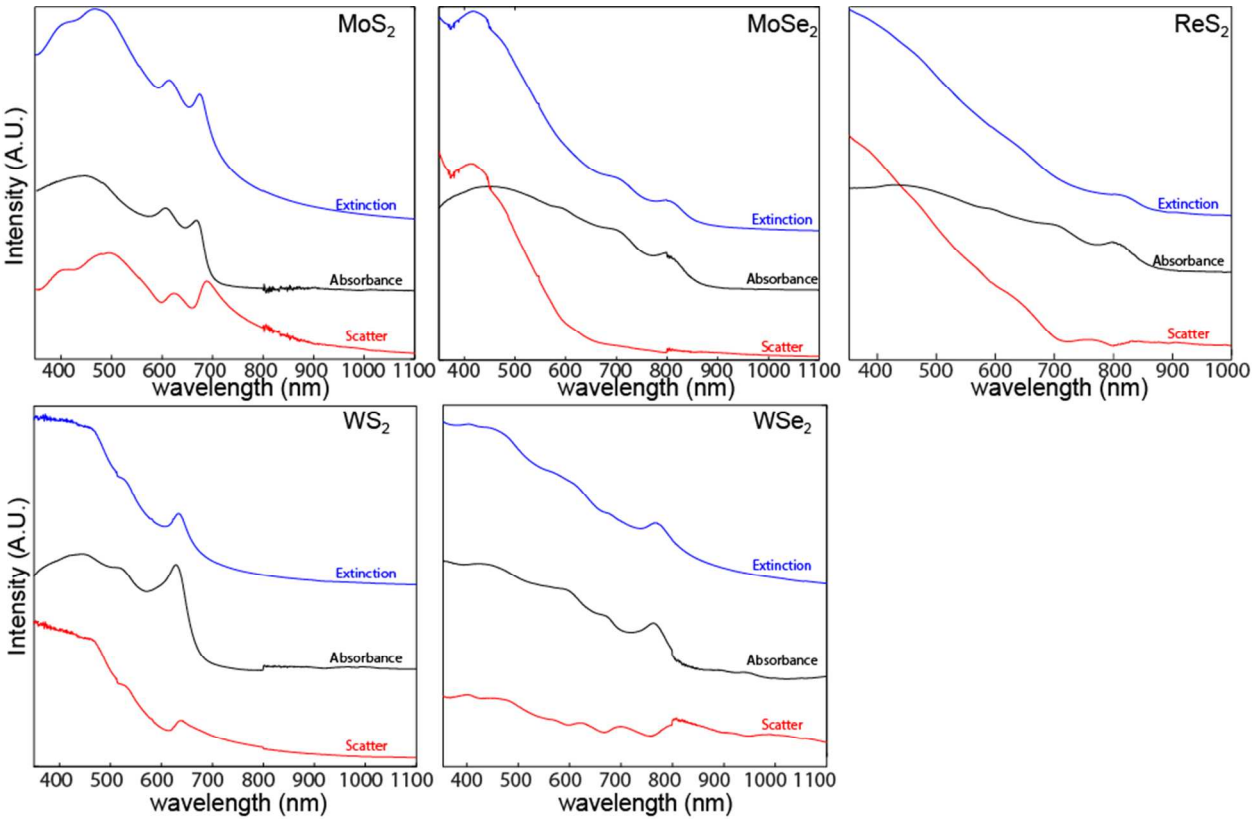

Figure S11. Extinction, Absorption, and Scattering profiles of TMDs. Scattering profile were obtained by subtracting extinction and absorption profiles from a single dispersion. Absorption spectra were obtained using an integrating sphere (Cary 5000). The scattering intensity is known to be size dependent, and spectra obtained for MoS_2 are similar to previously published results.[10] Note, $NbSe_2$ and $MoTe_2$ spectra are not shown. $NbSe_2$ is known to be metallic and thus has a negligible absorption spectra, and due to instrumentation limitations, the NIR $MoTe_2$ spectra could not be resolved in the integrating sphere.

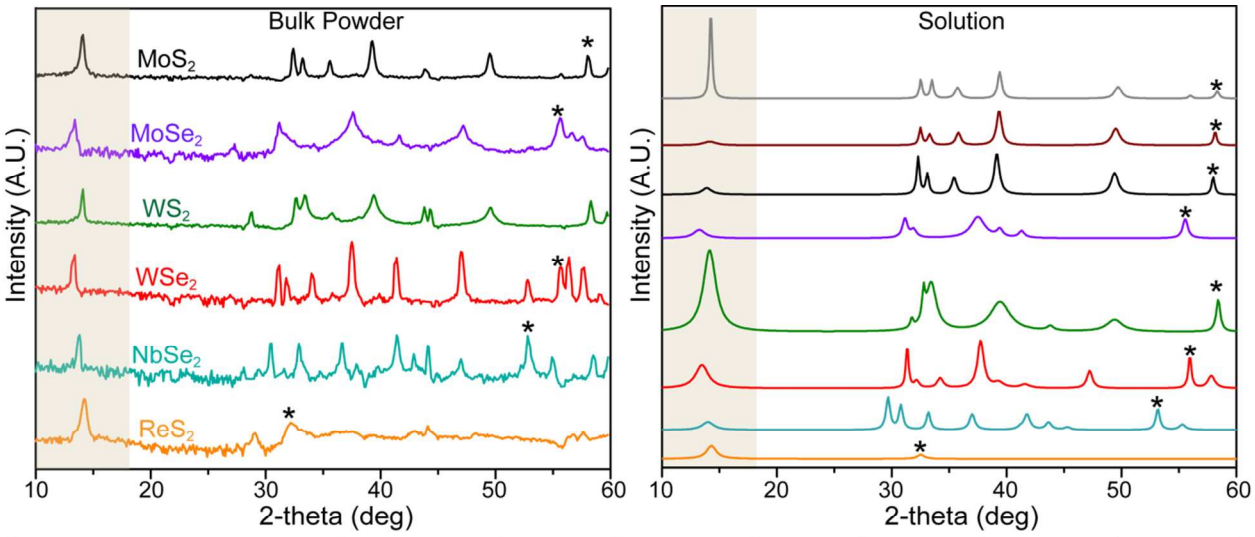

$\frac{I_{002}}{I_{110}}$	Probe-tip MoS_2	Redox MoS_2	$MoSe_2$	WS_2	WSe_2	$NbSe_2$	ReS_2
Exfoliated Solution	**0.21**	**0.24**	**0.29**	**0.56**	**0.45**	**0.26**	**0.75**
Bulk Powder	**0.80**	**0.80**	**0.48**	**0.68**	**0.69**	**0.47**	**0.82**

Figure S12. Bulk powder and solution phase XRD spectra of TMD dispersions. Bulk powder XRD are consistent with known crystallographic powder diffraction database: MoS_2 (PDF# 00-037-1492), $MoSe_2$ (PDF# 01-077-1715), $MoTe_2$ (PDF# 00-015-0658), WS_2 (PDF# 00-038-1388), WSe_2 (PDF# 00-038-1388), $NbSe_2$ (PDF# 00-019-0872), ReS_2 (PDF# 00-052-0818). The presence of [00*l*] (highlighted in beige) and [*hk0*](denoted with a star) reflections provide structural information about the TMD layers along the out-of-plane and in-plane directions respectively.[11,12] A decrease in intensity of the [002] reflection in solution as compared to bulk powder is indicative of a loss in correlation along the *c*-axis (stacking axis) and the intensity ratios of the [002]:[110] provides a quantitative assessment of the extent of exfoliation.[11] $\frac{I_{002}}{I_{110}} = 0$ is indicative of full exfoliation in solution. As a processing standard, liquid phase exfoliation of MoS_2 after 90 hours probe tip sonication is used to calibrate the redox exfoliation. For most samples, similar values for $\frac{I_{002}}{I_{110}}$ are obtained around 20-30% (MoS_2, $MoSe_2$, $NbSe_2$). WX_2 and ReS_2 exfoliates show higher values, which may be attributed to un-optimized oxidation/reduction conditions. Note the $\frac{I_{001}}{I_{2\bar{2}0}}$ is used for ReS_2 due to its triclinic unit cell.[13] In addition, the yield for $MoTe_2$ in solution is less than 1%, and thus the concentration was too dilute for XRD measurement, and it's spectra are omitted.

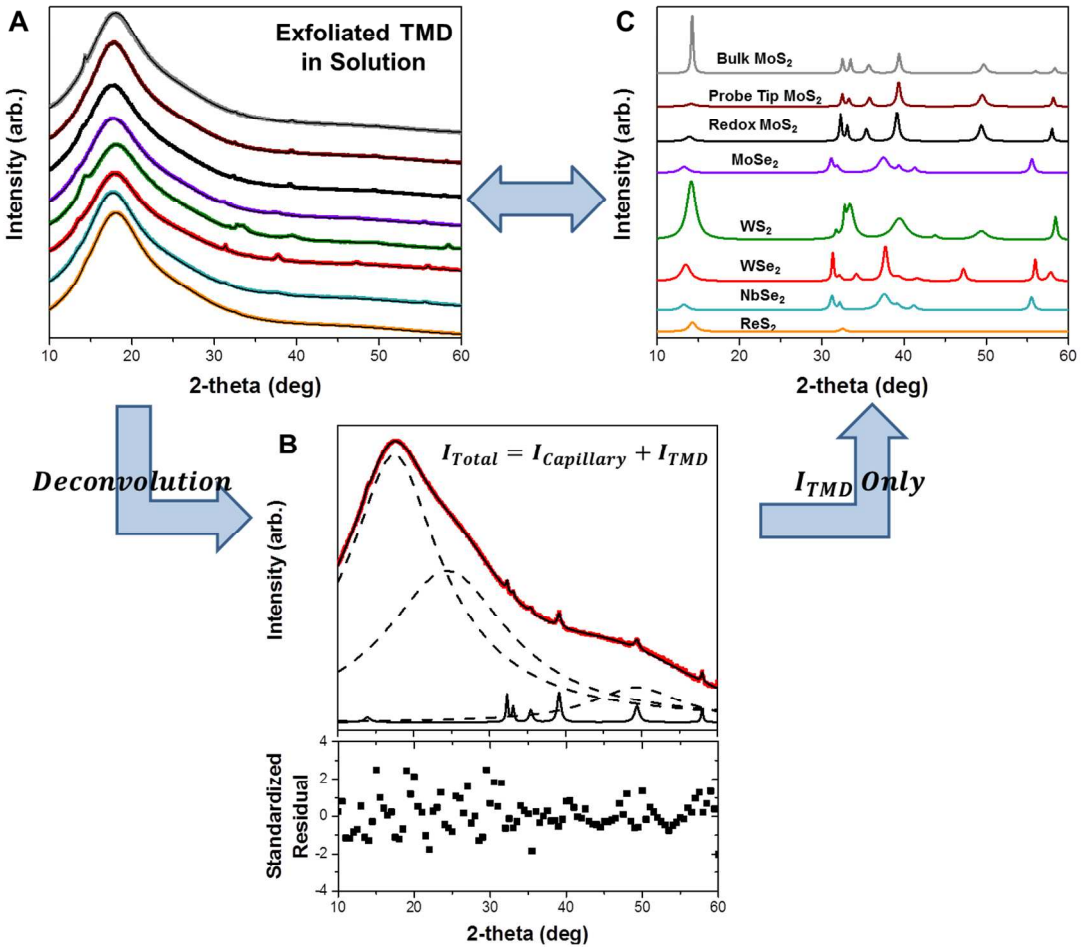

Figure S13. Data processing and fits for solution XRD spectra. **A)** Total scattering intensity of experimental (colored lines) and fits (solid black lines) for exfoliated TMDs in solution. It is to note that the total scattering intensity contains contributions from the TMD and the quartz capillary used to hold the solution. Background subtraction to isolate the TMD from the total intensity was difficult due to the strong scattering from the capillary (at 2θ=18°). Thus, the total intensity was deconvoluted using peak fitting methods in order to obtain the TMD scattering spectra. **B)** Peak deconvolution of the total scattering intensity for redox MoS_2. The total scattering intensity was deconvoluted into 3 capillary peaks (dashed lines) and TMD (solid black). The standardized residual was calculated by $\frac{I_{Fit}-I_{exp}}{\sigma}$, where σ is the standard deviation. The standardized residual plot shows a random distribution with no trends, which indicates a good fit with the experimental. **C)** Solution scattering spectra of TMD only obtained after peak deconvolution in **B** from total scattering intensity.

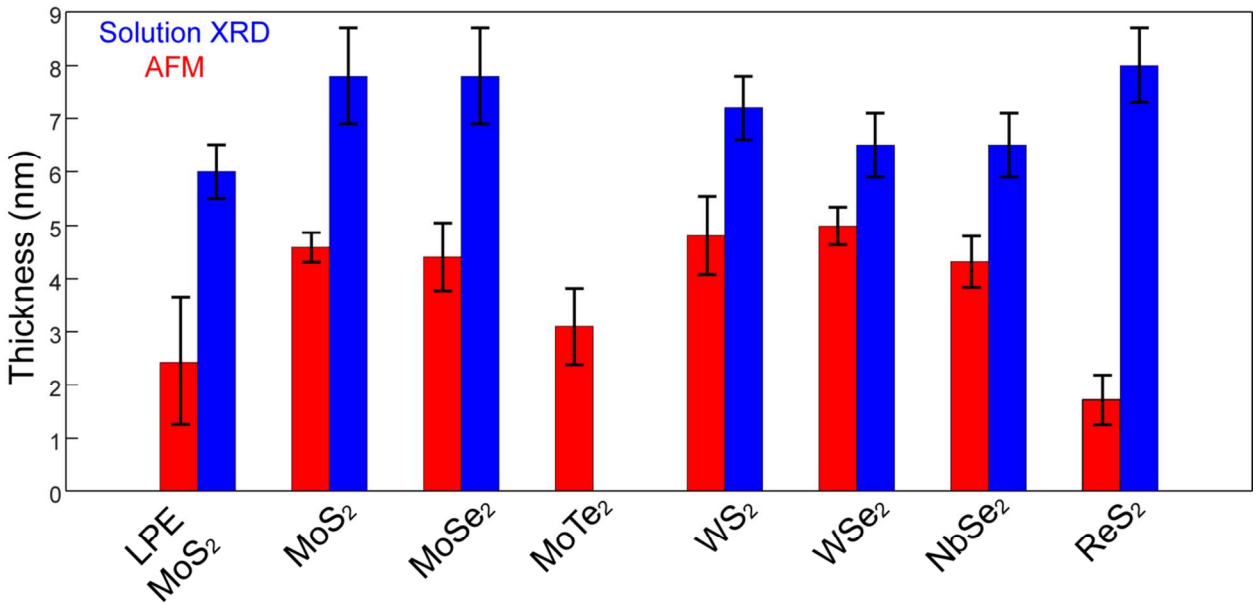

Figure S14. Height distributions obtained from AFM analysis show narrow size distributions ($\pm$ 1 – 2 monolayers) for all TMDs. Contrastingly, LPE of MoS_2 has a very broad size distribution ($\pm$4 layers). Scherrer analysis from solution XRD confirms similar thicknesses. It is to note that the crystallite sizes obtained from XRD reflect a global average, whereas selective local regions were analyzed via AFM. Thus, XRD overestimates the thicknesses of exfoliated flakes, while AFM/UV-Vis underestimate the total distribution.

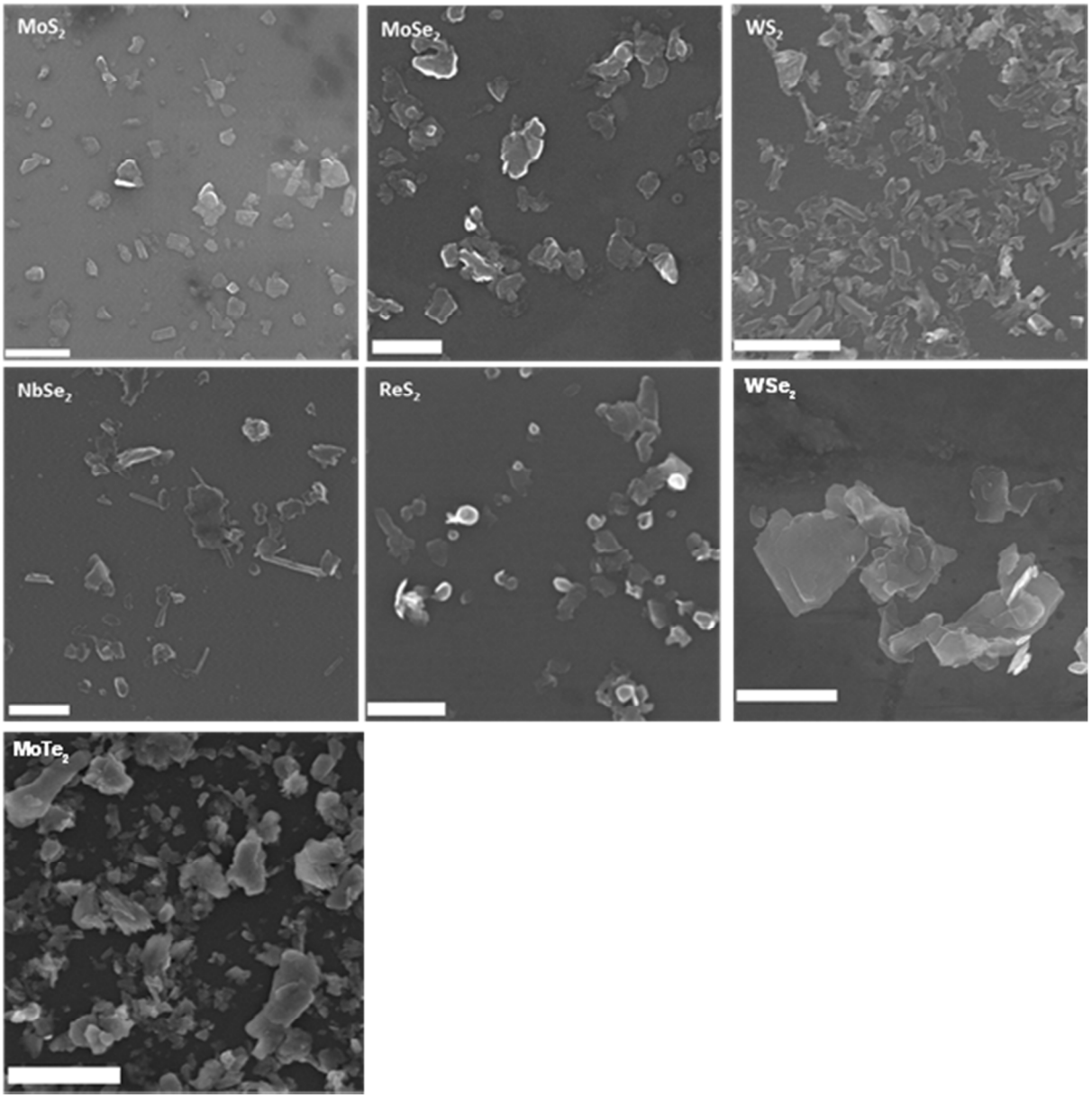

Figure S15. SEM micrographs of TMD flakes drop-cast on Si wafer showing few layer flakes. Scale bars: MoS_2, WS_2, ReS_2 200 nm; $MoSe_2$, $NbSe_2$ 300 nm; $MoTe_2$ 1 micron; WSe_2 2 micron. SEM microscopy indicates that flake diameters were correlated to the initial bulk powder used for exfoliation (see Table S2). For larger initial powders (> 10 micron), such as $MoSe_2$ and $MoTe_2$, exfoliated flakes were micron size, while for smaller bulk material (2 micron), such as MoS_2 and WS_2, exfoliated flakes were on the order of a few hundred nanometers, similar to sizes obtained via other bulk processing methods.

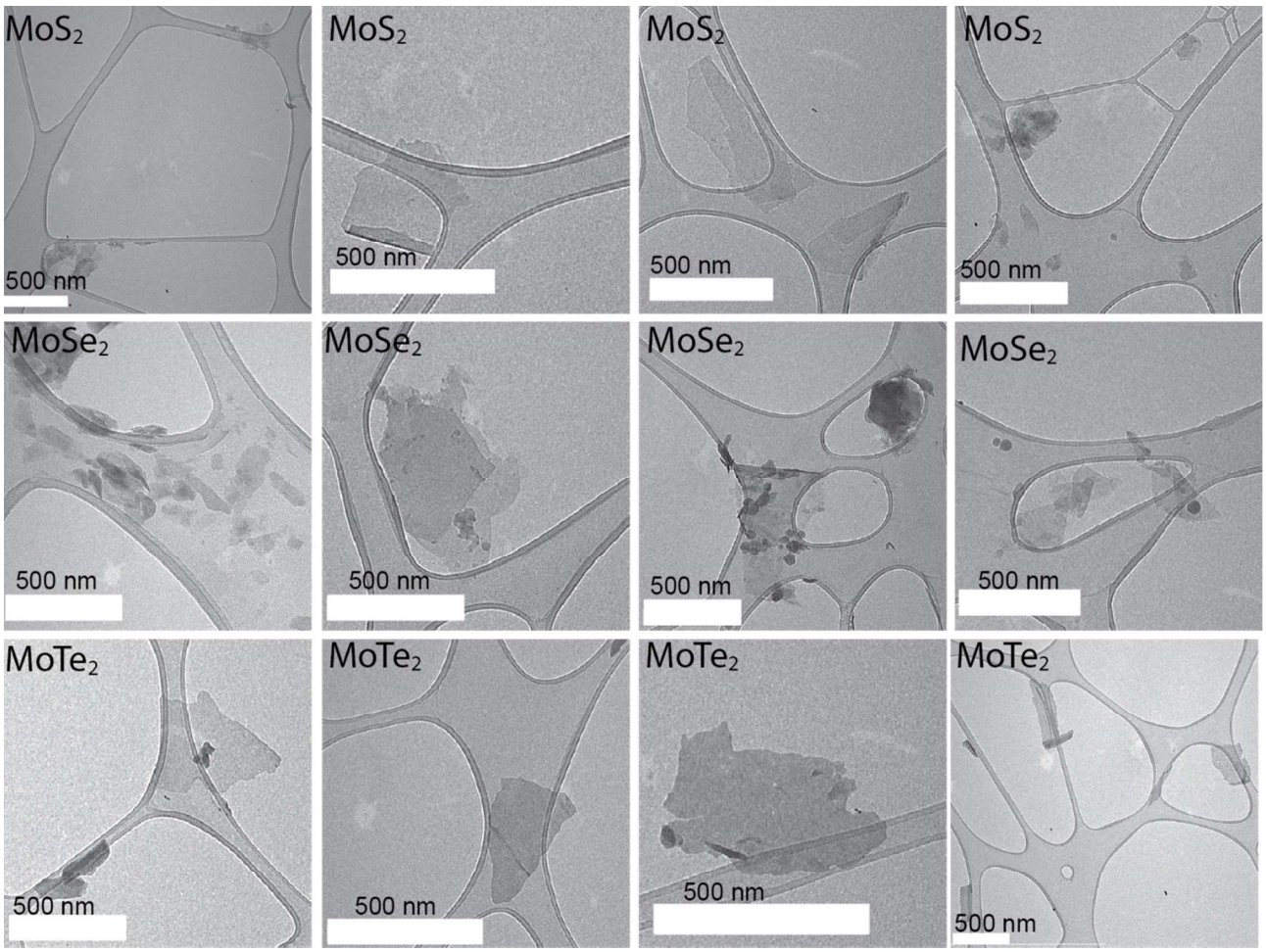

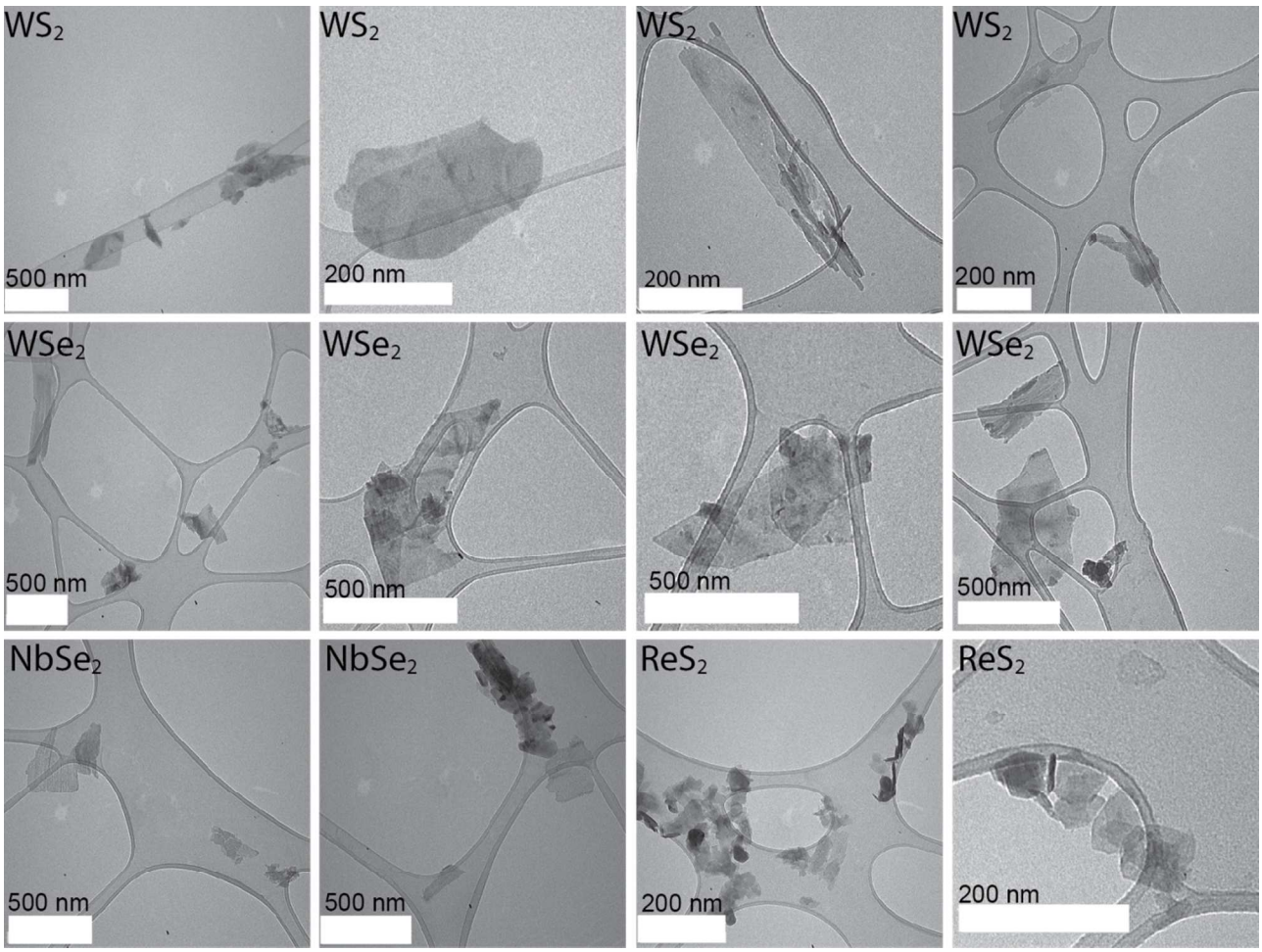

Figure S16. TEM images of flakes show transparent, thin flakes are obtained via Redox Exfoliation. Similar shapes and sizes are observed in SEM images (Figure S19) and AFM images (Figure 3, main text).

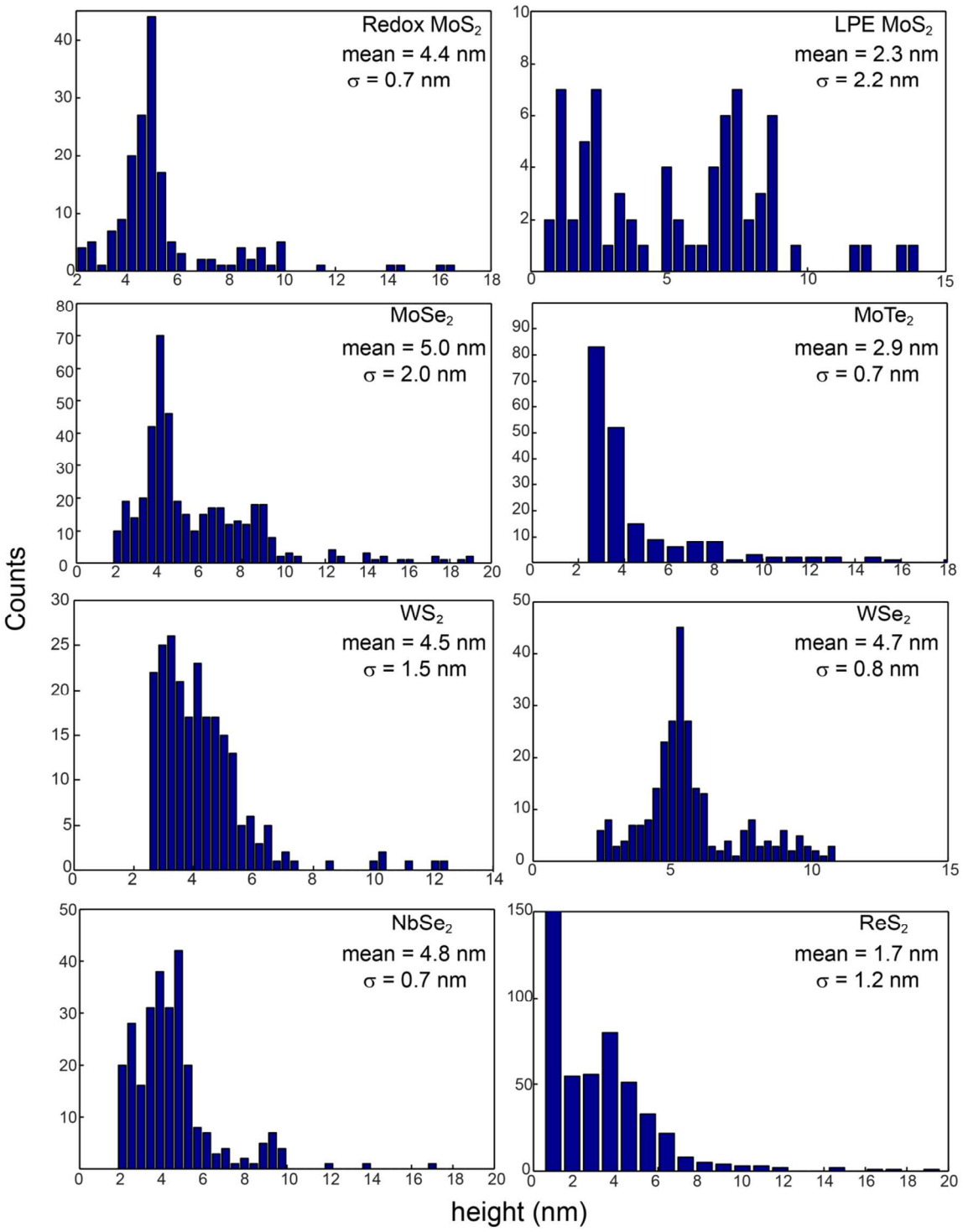

Figure S17. Height distributions obtained from AFM images. Note the narrow height profiles for TMDs exfoliated via redox method as compared to broad distributions of heights obtained from LPE exfoliation (90 hrs. continuous probe sonication, 0^{o}C). Mean distributions and standard deviations are summarized in Figure S11.

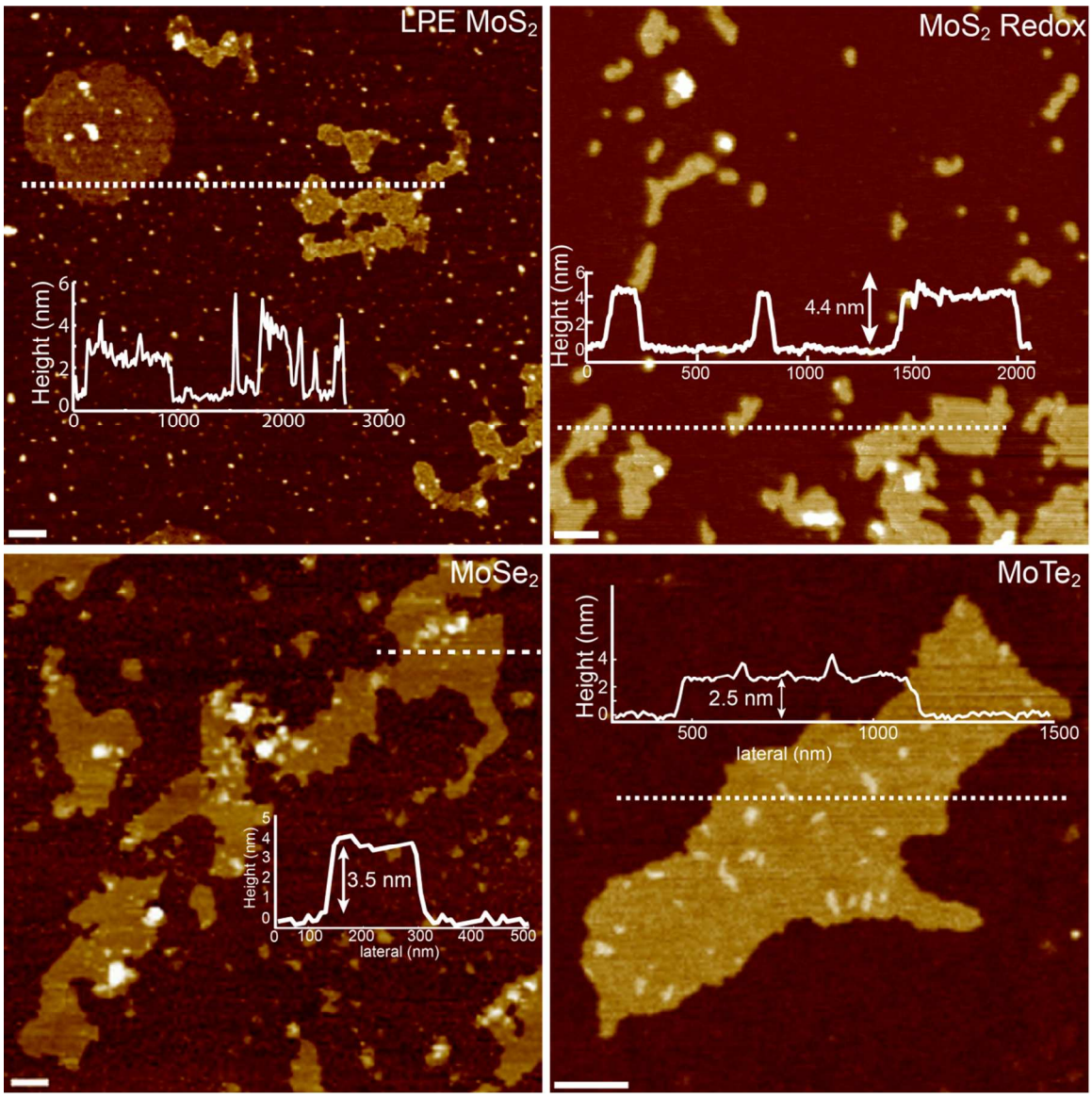

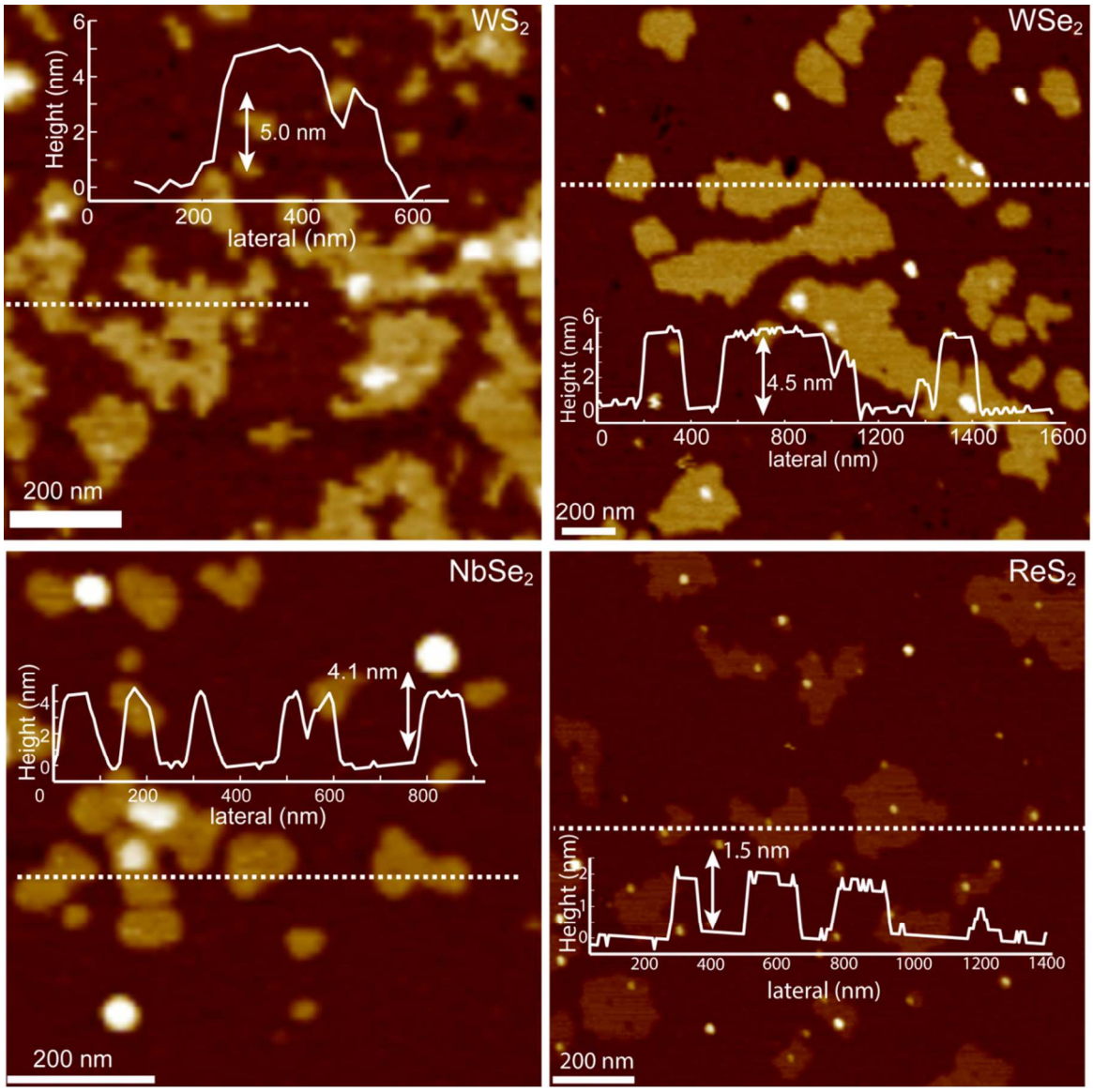

Figure S18. AFM images and line cuts of TMD flakes. Intermediate heights or steps were not observed for all samples. Small particulates (~1 nm thick) decorate the surface of ReS_2, $NbSe_2$, WSe_2, and $MoSe_2$. We believe these species to be POMs formed during redox reactions, as washing cycles remove these weakly bound species, as shown inshown in Figure S12.

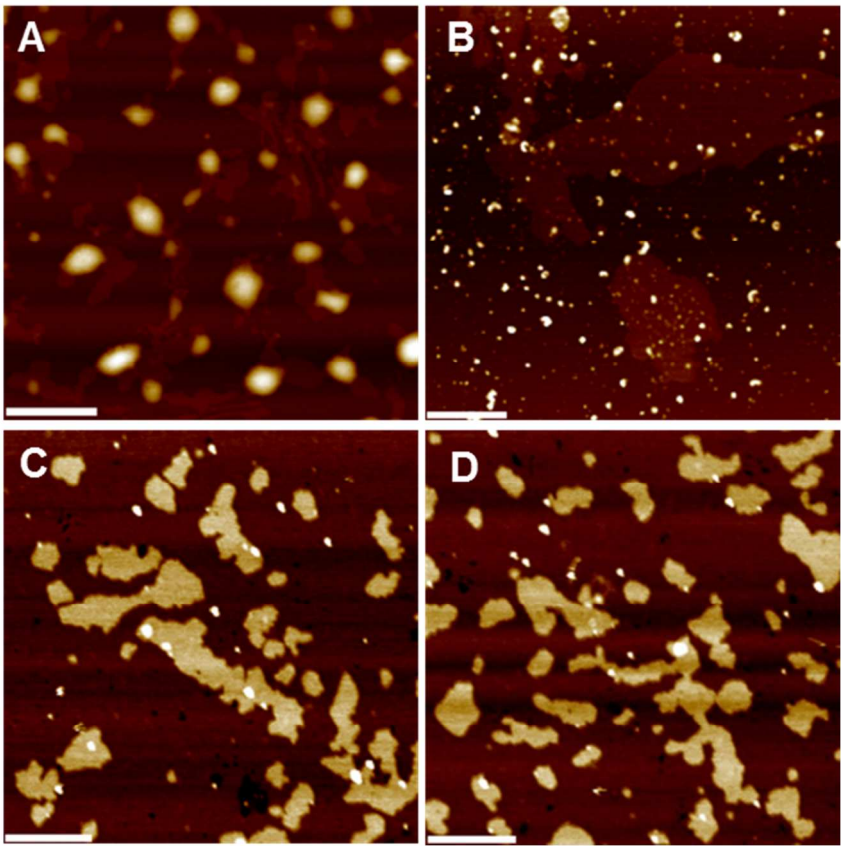

Figure S19. AFM images of WSe_2 before and after cleaning and re-dispersion. **A)** As prepared solution shows large species associated with the surface of WSe_2 flakes. **B)** After centrifugation and removal of solvent, followed by redispersion in acetonitrile (1x cleaning), the surface species become smaller, until finally **C,D**) they are removed almost entirely after another round of centrifugation and redispersion in fresh solvent (2x cleaning). Scale bars for **A** and **B** are 1 micron. Scale bars for **C** and **D** are 500 nm.

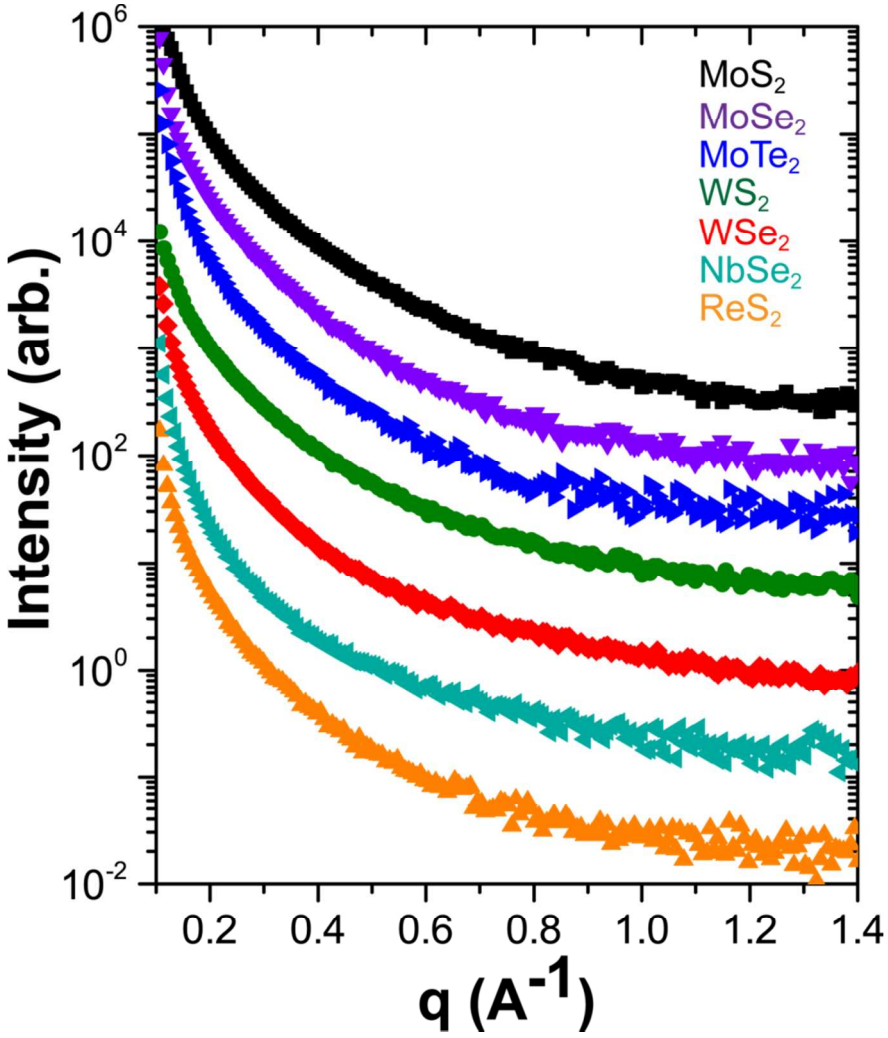

Figure S20. SAXS reflection of thin films of exfoliated TMDs. The presence of intercalated structures would emerge as larger spacings along the [002] crystallographic axis. Intercalation compounds increase the *c*-axis crystallite size.[14–16] SAXS spectra on drop-cast exfoliated TMD solutions show no evidence for intercalated structures formed with *d*-spacings less than 4.5 nm. Due to this null result, we do not believe that intercalation is a driving mechanism for exfoliation. It is to note that the scattering peak at q=1.32 A^{-1} (d-spacing=4.8 A) for $NbSe_2$ is also present in the bulk powder sample, which may be attributed to impurities present in the sample.

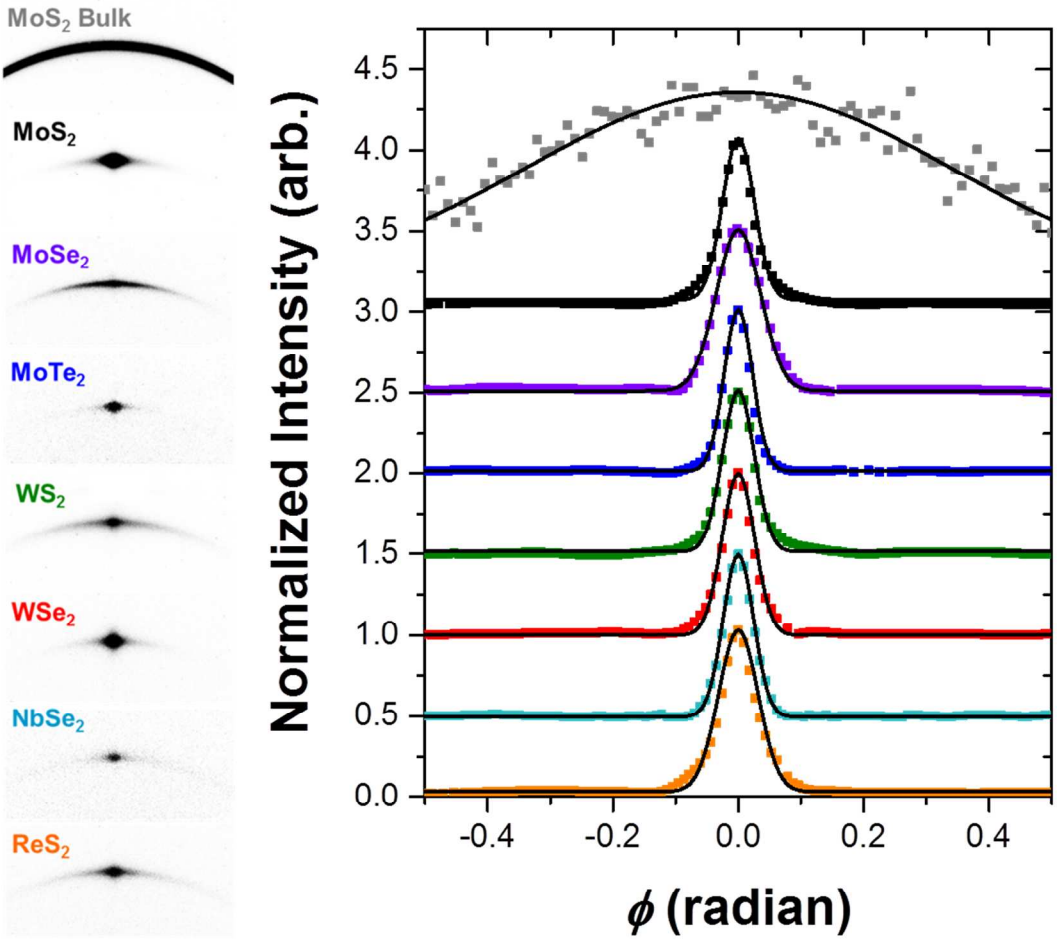

Figure S21. Orientation analysis of exfoliated flakes drop cast onto Si wafers. 2D XRD scans of the exfoliated TMDs along the (002) crystallographic axis (left). Azimuthal plots of the 2D XRD scans (right) with calculated Hermans' orientation parameters (solid black lines). A P_2~0 was obtained for bulk MoS2 (random orientation of flakes), whereas P2~0.7-0.9 was obtained for all the exfoliated TMDs (high orientation of flakes stacked along the c-axis.)

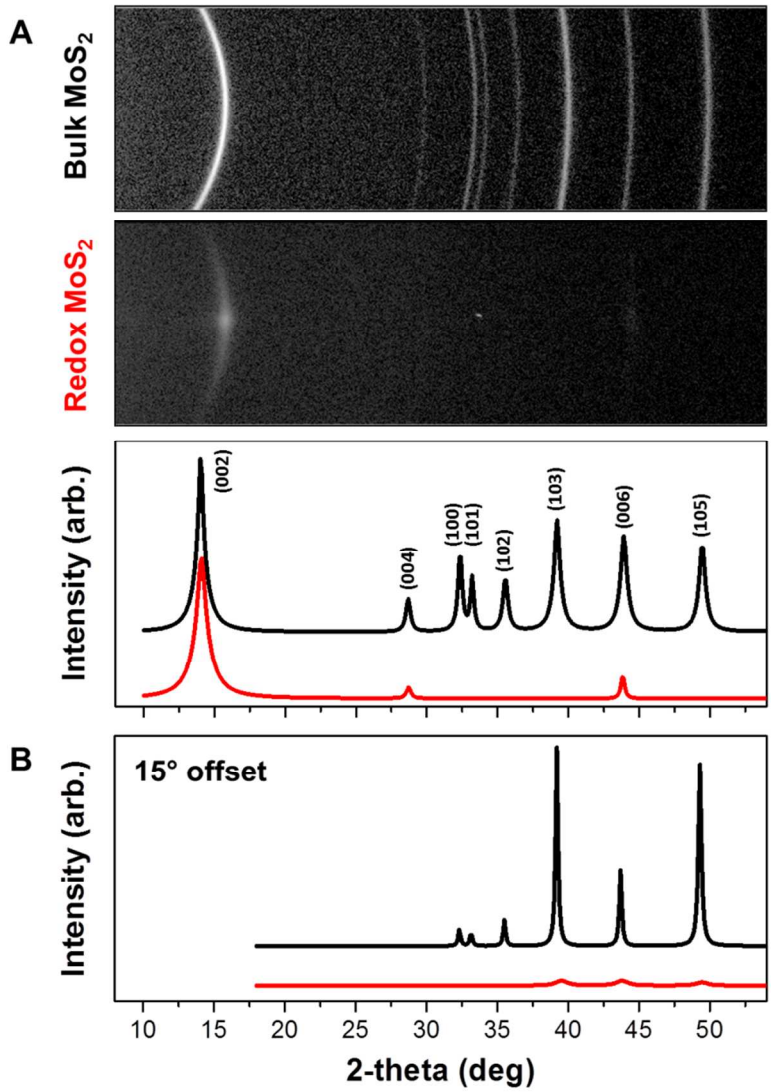

Figure S22. **A)** 2D XRD pattern of bulk (black) and redox (red) thin films of MoS_2. The disappearance of the [*hk*0] and [*h*0*l*] reflections confirms exfoliation of TMDs in solution and restacking along the [00*l*] axis during film formation. **B)** The sample was set at an offset incline in order to confirm the removal of the [*h*0*l*] reflections observed in **A**. The angle between the [002] and [103] plane is ~18°, thus, the intensity of the [103] reflection was optimized by tilting the sample at 15°. It is to note that data points less than 2θ=18° cannot be obtained due to the offset incline. Although the [103] and [105] reflections can be observed in the redox sample, the intensities are extremely weak and significantly reduced as compared to the bulk, which is indicative of a turbostratic structure with stacking faults along the [002] axis.

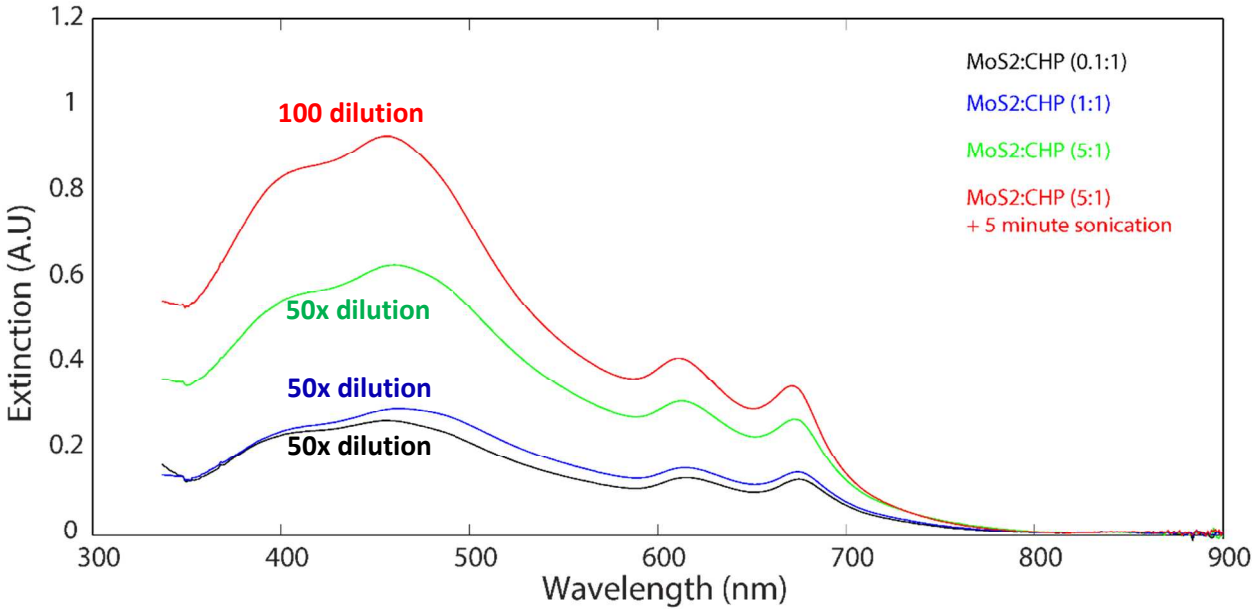

Figure S23. UV-Vis extinction spectra of MoS_2 exfoliation as a function of CHP addition. Constant amounts of $NaBH_4$ were added (400 μmol). Initially, low loading ratios of CHP (0.1:1, 1:1) give low yields, while a ratio of 5:1 increases yields approximately 3 fold. Addition of 30 minutes of sonication further increases the yields 2x compared to samples prepared without sonication.

TMD	Bulk Powder size (μm)	Lateral dimension (exfoliated, nm)	Initial mass (mg)	Mass suspended (mg)	% suspended	% exfoliated
LPE MoS_2	2	149 ± 61	30	N/A	N/A	3
Redox MoS_2	2	224 ± 126	30	23 – 28	66 – 90	5 – 10
$MoSe_2$	44	232± 211	30	6.1	20	2
$MoTe_2$	10	405 ± 209	30	< 1	N/A	N/A
WS_2	N/A	325 ± 75	30	3.1	10.3	1
WSe_2	N/A	418 ± 59	30	4.1	13.6	4
$NbSe_2$	N/A	210 ± 128	30	15.5	51	5
ReS_2	N/A	121 ± 49	30	30	100	10

Table S1. Summary of bulk particle size, exfoliated flake dimensions, % yield of suspended flakes, and % yield of exfoliated flakes. After redox reactions, the mass of suspended flakes was determined by pipetting out a known aliquot from the reaction vessel after the stir was removed and large, unsuspended flakes were sedimented. The aliquot was centrifuged at 10000 RPM, washed several times with CH_3CN to remove excess $NaBH_4$ and CHP in the vessel, and then transferred to a pre-weighed vial. The solvent was removed at 60^oC under vacuum (200 mTorr) and the vial re-weighed. The mass difference is reported as the suspended flake mass. These contain both exfoliated flakes as well as non-exfoliated, bulk flakes. Exfoliated %'s were determined by carrying out a size selection centrifugation step to separate out large, un-exfoliated material with thin, exfoliated flakes. These values are generally much smaller than suspended masses/yields. Masses were measured by difference after removal of solvent under vacuum (300 mTorr).

TMD	a (nm)	c (nm)	[100] (nm)	[110] (nm)	[111] (nm)	[200] (nm)
MoS2	3.15	12.30	2.72	1.57	1.56	1.92
MoSe2	3.28	12.93	2.84	1.64	1.62	2.00
MoTe2	3.55	13.86	3.07	1.77	1.76	2.17
WS2	3.18	12.32	2.75	1.59	1.57	1.94
WSe2	3.29	12.98	2.84	1.64	1.63	2.01
NbSe2	3.6	12.60	3.11	1.81	1.78	2.20
ReS2	6.45	6.40	5.58	3.22	2.88	3.94

Table S2. [100], [110] and [111] diffraction planes for TMDs obtained from HRTEM *a* and *c* lattice parameters. When possible, the [200] and [111] diffraction peaks were analyzed. All identified peaks were within 5% error of actual spacings.

$[MoS_2]$ (mg/mL)	mmol CHP	μmol $NaBH_4$	$[MoS_2]$ suspended (mg/mL)	$[MoS_2]$ exfoliated (μg/mL)
3	0.01	400	0.05 (15%)	18 (0.6%)
3	0.1	400	1.44 (48%)	165 (5%)
3	1	400	2.57 (88%)	278 (9.2%)
3	10	400	0.49 (16%)	N/A
3*	1*	400*	2.85*	455*

*sample was probe sonicated (30 min, 125 W) after redox reaction was performed.

Table S3. Summary of MoS_2 suspension and exfoliation yields. Reactions were carried out at 0^oC, and allowed to react for 24 hours after CHP addition, and another 24 hours after aqueous 0.10 M $NaBH_4$ addition which was added in 100 μL increments in 60 minute intervals. All reactions performed under argon atmosphere and with anhydrous solvents

References:

(1) Ammam, M. Polyoxometalates: Formation, Structures, Principal Properties, Main Deposition Methods and Application in Sensing. *J. Mater. Chem. A* **2013**, *1*, 6291–6312.

(2) Long, D. L.; Tsunashima, R.; Cronin, L. Polyoxometalates: Building Blocks for Functional Nanoscale Systems. *Angew. Chemie - Int. Ed.* **2010**, *49*, 1736–1758.

(3) Khenkin, A. M.; Leitus, G.; Weiner, L.; Neumann, R. The Synthesis and Characterization of the Tri-rhenium(VI) Capped Wells--Dawson Polyoxometalate, [{}(C4H9)4N)5(C2H5)3NH{}}{{}Re3P2W15O62{}}]. *J. Clust. Sci.* **2014**, *25*, 687–693.

(4) Chen, Q.; Zubieta, J. Synthesis and Structural Characterization of a Polyoxovanadate Coordination Complex with a Hexametalate Core: [(N-C4H9)4N]2[V6O13{O2NC(CH2O)3}2]. *Inorg. Chem.* **1990**, *29*, 1456–1458.

(5) Nyman, M. Polyoxoniobate Chemistry in the 21st Century. *Dalton Trans.* **2011**, *40*, 8049–8058.

(6) Zhou, Z.-H.; Hou, S.-Y.; Wan, H.-L. Peroxomolybdate(VI)-Citrate and -Malate Complex Interconversions by pH-Dependence. Synthetic, Structural and Spectroscopic Studies. *Dalton Trans.* **2004**, 1, 1393–1399.

(7) Bonchio, M.; Conte, V.; Furia, F. Di; Carofiglio, T.; Magno, F.; Pastore, P. CoII-Induced Radical Oxidations by Peroxomolybdenum Complexes. *J. Chem. Soc. Perkin Trans.* **1993**, 2, 1923–1926.

(8) Müller, A.; Meyer, J.; Krickemeyer, E.; Diemann, E. Molybdenum Blue: A 200 Year Old Mystery Unveiled. *Angew. Chemie Int. Ed. English* **1996**, *35*, 1206–1208.

(9) Krebs, B.; Droste, E.; Piepenbrink, M. Syntheses and Crystal Structure Studies of Novel Selenium- and Tellurium-Substituted Lacunary Polyoxometalates. In *Polyoxometalate Chemistry From Topology via Self-Assembly to Applications*; Pope, M. T., Müller, A., Eds.; Springer Netherlands: Dordrecht, 2001; pp 89–99.

(10) Backes, C.; Smith, R. J.; McEvoy, N.; Berner, N. C.; McCloskey, D.; Nerl, H. C.; O'Neill, A.; King, P. J.; Higgins, T.; Hanlon, D.; Scheuschner, N.; Maultzsch, J.; Houben, L.; Duesberg, G. S.; Donegan, J. F.; Nicolosi, V.; Coleman, J. N. Edge and Confinement Effects Allow in Situ Measurement of Size and Thickness of Liquid-Exfoliated Nanosheets. *Nat. Commun.* **2014**, *5*, 4576.

(11) Nguyen, Q. T.; Baird, D. G. An Improved Technique for Exfoliating and Dispersing Nanoclay Particles into Polymer Matrices Using Supercritical Carbon Dioxide. *Polymer (Guildf).* **2007**, *48*, 6923–6933.

(12) Burnside, S. D.; Giannelis, E. P. Synthesis and Properties of New Poly(dimethylsiloxane) Nanocomposites. *Chem. Mater.* **1995**, *7*, 1597–1600.

(13) Fujita, T.; Ito, Y.; Tan, Y.; Yamaguchi, H.; Hojo, D.; Hirata, A.; Voiry, D.; Chhowalla, M.; Chen, M. Chemically Exfoliated ReS2 Nanosheets. *Nanoscale*

2014, *6*, 12458–12462.

(14) Whittingham, M. S. *Intercalation Chemistry*; 1982.

(15) Benavente, E.; Santa Ana, M. a.; Mendizábal, F.; González, G. Intercalation Chemistry of Molybdenum Disulfide. *Coord. Chem. Rev.* **2002**, *224*, 87–109.

(16) Dines, M. B. Lithium Intercalation via -Butyllithium of the Layered Transition Metal Dichalcogenides. *Mater. Res. Bull.* **1975**, *10*, 287–291.